PLOS | PATHOGENS

RESEARCH ARTICLE

Humoral immune response to adenovirus induce tolerogenic bystander dendritic cells that promote generation of regulatory T cells

Thi Thu Phuong Tran[1], Karsten Eichholz[1¤], Patrizia Amelio[2], Crystal Moyer[3], Glen R. Nemerow[3], Matthieu Perreau[2], Franck J. D. Mennechet[1], Eric J. Kremer[1]*

1 Institut de Génétique Moléculaire de Montpellier, University of Montpellier, CNRS, Montpellier, France, **2** Division of Immunology & Allergy, University of Lausanne, Lausanne, Switzerland, **3** Department of Immunology and Microbial Science the Scripps Research Institute, La Jolla, CA, United States of America

¤ Current address: Vaccine and Infectious Disease Division, Fred Hutchinson Cancer Research Center, Seattle, WA, United States of America
* eric.kremer@igmm.cnrs.fr

Citation: Tran TTP, Eichholz K, Amelio P, Moyer C, Nemerow GR, Perreau M, et al. (2018) Humoral immune response to adenovirus induce tolerogenic bystander dendritic cells that promote generation of regulatory T cells. PLoS Pathog 14(8): e1007127. https://doi.org/10.1371/journal.ppat.1007127

Editor: Patrick Hearing, Stony Brook University, UNITED STATES

Received: May 25, 2018

Accepted: July 3, 2018

Published: August 20, 2018

Data Availability Statement: All relevant data are within the paper and its Supporting Information files.

Funding: This study was funded through the Marie Sklodowska-Curie actions initial training network (FP7 ITN; ADVance #290002) (EJK), the Agence Nationale de la Recherche (ANR, DCTaxis) (EJK), Swiss National Science Foundation (#320030_173071) (MP), the Labex EpiGenMed (EJK), an ANR "Investissements d'avenir" program,

Abstract

Following repeated encounters with adenoviruses most of us develop robust humoral and cellular immune responses that are thought to act together to combat ongoing and subsequent infections. Yet in spite of robust immune responses, adenoviruses establish subclinical persistent infections that can last for decades. While adenovirus persistence pose minimal risk in B-cell compromised individuals, if T-cell immunity is severely compromised reactivation of latent adenoviruses can be life threatening. This dichotomy led us to ask how anti-adenovirus antibodies influence adenovirus T-cell immunity. Using primary human blood cells, transcriptome and secretome profiling, and pharmacological, biochemical, genetic, molecular, and cell biological approaches, we initially found that healthy adults harbor adenovirus-specific regulatory T cells (T_{regs}). As peripherally induced T_{regs} are generated by tolerogenic dendritic cells (DCs), we then addressed how tolerogenic DCs could be created. Here, we demonstrate that DCs that take up immunoglobulin-complexed (IC)-adenoviruses create an environment that causes bystander DCs to become tolerogenic. These adenovirus antigen loaded tolerogenic DCs can drive naïve T cells to mature into adenovirus-specific T_{regs}. Our study reveals a mechanism by which an antiviral humoral responses could, counterintuitively, favor virus persistence.

Author summary

While numerous studies have addressed the cellular and humoral response to primary virus encounters, relatively little is known about the interplay between persistent infections, neutralizing antibodies, antigen-presenting cells, and T-cell responses. Our studies suggests that if adenovirus–antibody complexes are taken up by professional antigen-presenting cells (e.g. dendritic cells), the DCs can generate an environment that causes bystander dendritic cells to become tolerogenic. These tolerogenic dendritic cells favors

(ANR-10-LABX-12-01) (EJK), the Université de Montpellier (Soutien a la Recherche) (EJK), Vietnamese Minister of Education (TTPT), the Innovative Medicine Initiative EboVac2 (#115861) (EJK), and L'institut de Génétique Moléculaire de Montpellier (EJK). EJK is an Inserm fellow. The funders had no role in study design, data collection and analysis, decision to publish, or preparation of the manuscript.

Competing interests: The authors have declared that no competing interests exist.

the creation of adenovirus-specific regulatory T cells. While this pathway likely favors pathogen survival, there may be advantages for the host also.

Introduction

Human adenoviruses (HAdVs), of which there may be 85 types (based on serology and genome analyses), typically cause self-limiting respiratory, ocular, and gastro-intestinal tract infections in immunocompetent individuals. After repeated encounters, most young adults generally harbor cross-reactive, long-lived humoral and T-cell responses [1–3] that are thought to work together to efficiently blunt subsequent HAdV-induced morbidity. However, in spite of the robust anti-HAdV immune responses, HAdVs routinely establish decades-long, subclinical infections that are characterized by low level shedding of progeny virions [4,5]. While potential molecular mechanisms by which HAdVs evade the immune response have been proposed [6], we suspected that complementary mechanisms also exist. Of note, in T-cell compromised patients the loss of cellular control of persistent HAdV infection can lead to fulminant and fatal disease [4,5]. It is noteworthy that serological evidence that the patient has been infected by a given HAdV type before hematopoietic stem cell transplantation is predictive of escape from the same HAdV type during immune suppression [7].

While T-cell therapy has shown a notable potential to prevent HAdV disease in immunocompromised patients [8,9], immunoglobulin therapy has had remarkably little impact [4]. Due to omnipresent anti-HAdV antibodies, it is not surprising that immunoglobulin-complexed HAdVs (IC-HAdVs) are detected in some patients with HAdV disease [10–12]. In a broader view, immunoglobulin-complexed viruses can form during prolonged viremia, secondary infections, primary infections when a cross-reactive humoral response exists, and in the presence of antibody-based antiviral therapy. It is important to note that IC-HAdVs are potent stimulators of human dendritic cell (DC) maturation [13,14]. In immunologically naïve hosts, immunoglobulin-complexed antigens are efficient stimulators of antibody and cytotoxic T-cell responses [15]. However, most studies using immunoglobulin-complexed antigens have used prototype antigens that have little impact on their intracellular processing. This is not the case for IC-HAdVs. The endosomolytic activity of protein VI, an internal capsid protein, prevents the canonical processing of the IC-HAdVs by enabling the escape of HAdV capsid and its genome from endosomes into the cytoplasm [14]. In the cytoplasm, the HAdV genomes are detected by absent in melanoma 2 (AIM2), a cytosolic pattern recognition receptor (PRR) [16]. AIM2 engagement of the 36 kb HAdV-C5 genome induces pyroptosis, a pro-inflammatory cell death in conventional DCs [17]. Pyroptosis entails inflammasome formation, caspase 1 recruitment/auto-cleavage/activation, pro-IL-1β processing, gasdermin D (GSDMD) cleavage, GSDMD-mediated loss of cell membrane integrity, and IL-1β release [18,19].

Just as immune responses need to be initiated, suppression of cellular responses are primordial to avoid excessive tissue damage and feature prominently in acute and chronic infection [20–22]. Control of antigen-specific T cells can be mediated in part by peripherally induced antigen-specific regulatory T cells (T_{regs}) [23], which can favor the establishment of persistent viral infections. Moreover, tolerogenic DCs are required for antigen-specific T_{reg} formation. The variable phenotype and functionality of tolerogenic DCs are globally characterized by a semi-mature profile encompassing cell surface costimulatory molecules, cytokine expression and secretion, and antigen uptake and processing [24,25].

The goals of our studies were to determine how anti-HAdV humoral immunity impacts the cellular response to HAdVs, and whether this might affect persistence. Initially, we found that

healthy adults harbor HAdV-specific T_{regs}. We then demonstrated that IC-HAdV5-challenged human DCs induce a tolerogenic phenotype in bystander DCs. We show that the bystander DCs are capable of taking up and presenting HAdV antigens, and can drive naïve T cells to mature into HAdV-specific T_{regs}. Our study reveals a mechanism by which an antiviral humoral responses could, counterintuitively, favor virus persistence.

Results

HAdV-specific T_{regs} in healthy donors dampen HAdV-specific T cell proliferation

Initially, we asked if healthy adults harbor HAdV-specific T_{regs} and if so, are they capable of dampening anti-HAdV T-cell proliferation. To address these questions, we pre-screened a cohort of healthy individuals using an IFN-γ ELISpot assay for a memory T-cell response to HAdVs using a pool of overlapping HAdV5 hexon peptides (hexon is the major protein in the HAdV capsid). It is important to note that the anti-HAdV T-cell response is not species—or type-specific as the hexon sequence is highly conserved among all HAdVs. While the majority of 58 donors in this assay had a HAdV-specific T-cell response, PBMCs from 11 individuals with a spot forming unit ratio 5-fold greater than mock-treated cells were selected for further analyses. Because inducible T_{regs} can produce IL-10 in response to their cognate antigen, the ability of HAdV-specific $CD4^+$ T cells to produce IL-10 as well as IFN-γ, TNF, and IL-2 was assessed by multi-parametric flow cytometry. Consistent with our previous results [13], the cytokine profile of HAdV-specific memory $CD4^+$ T cells was dominated by polyfunctional IFN-γ^+/IL-2^+/TNF^+/IL-10^- cells (approximately 25% of total HAdV-specific $CD4^+$ T cells) and IFN-γ^+/IL-2^-/TNF^-/IL-10^- cells (approximately 20%) (**Fig 1A**, a representative donor). We then characterized the combinations of the responses and the percentage of functionally distinct populations in all donors (**Fig 1B**). Each slice of the pie chart corresponds to HAdV-specific $CD4^+$ T cells with a given number of functions, within the responding T-cell population. Of note, IL-10-producing HAdV-specific $CD4^+$ T cells, which were approximately 5% of total, were predominantly IFN-γ^-/IL-2^-/TNF^-. To determine if the IL-10 producing T cells have a T_{reg} phenotype, the expression of conventional T_{reg} markers, CD45RO, CD25, FoxP3, and CD127 [26], were assessed. We found that approximately 8% of the IL-10 producing T cells were $CD25^+$/$FoxP3^+$/$CD127^{dim}$. By contrast, most of IFN-γ producing HAdV-specific $CD4^+$ T cells harbored a conventional memory phenotype (CD45RO^+/$FoxP3^-$/$CD25^-$/$CD127^+$) (**Fig 1C**). These data demonstrate the presence of HAdV-specific T_{regs} in healthy adults.

To determine if putative HAdV-specific T_{regs} have regulatory functions, we used PBMCs from 5 individuals that harbored an anti-HAdV T-cell response. The CFSE-labeled PBMCs, or CFSE-labeled PBMCs depleted in CD25-expressing cells, were incubated with HAdV5 or the hexon peptide pool and T-cell proliferation was quantified. We found that depletion of $CD25^+$ cells caused $CD4^+$ cells to proliferate greater than control peptide-challenged $CD4^+$ cells (**Fig 1D**), suggesting that the HAdV-specific T_{regs} in the $CD25^+$ population can restrict the proliferative anti-HAdV T cells. Taken together, these data indicate that a fraction of HAdV-specific $CD4^+$ T cells harbors an inducible T_{reg} phenotype, and that healthy adults likely have $CD25^+$ T_{regs} that dampen the proliferation of HAdV-specific T cells.

Phenotypic maturation of bystander DCs

A prerequisite for antigen-specific T_{reg} formation is the presence of antigen-presenting tolerogenic DCs [27,28]. Because the cellular profile of HAdV5-challenged DC [29] is inconsistent with that of tolerogenic DCs [29], we asked if IC-HAdV5 could be involved in the generation

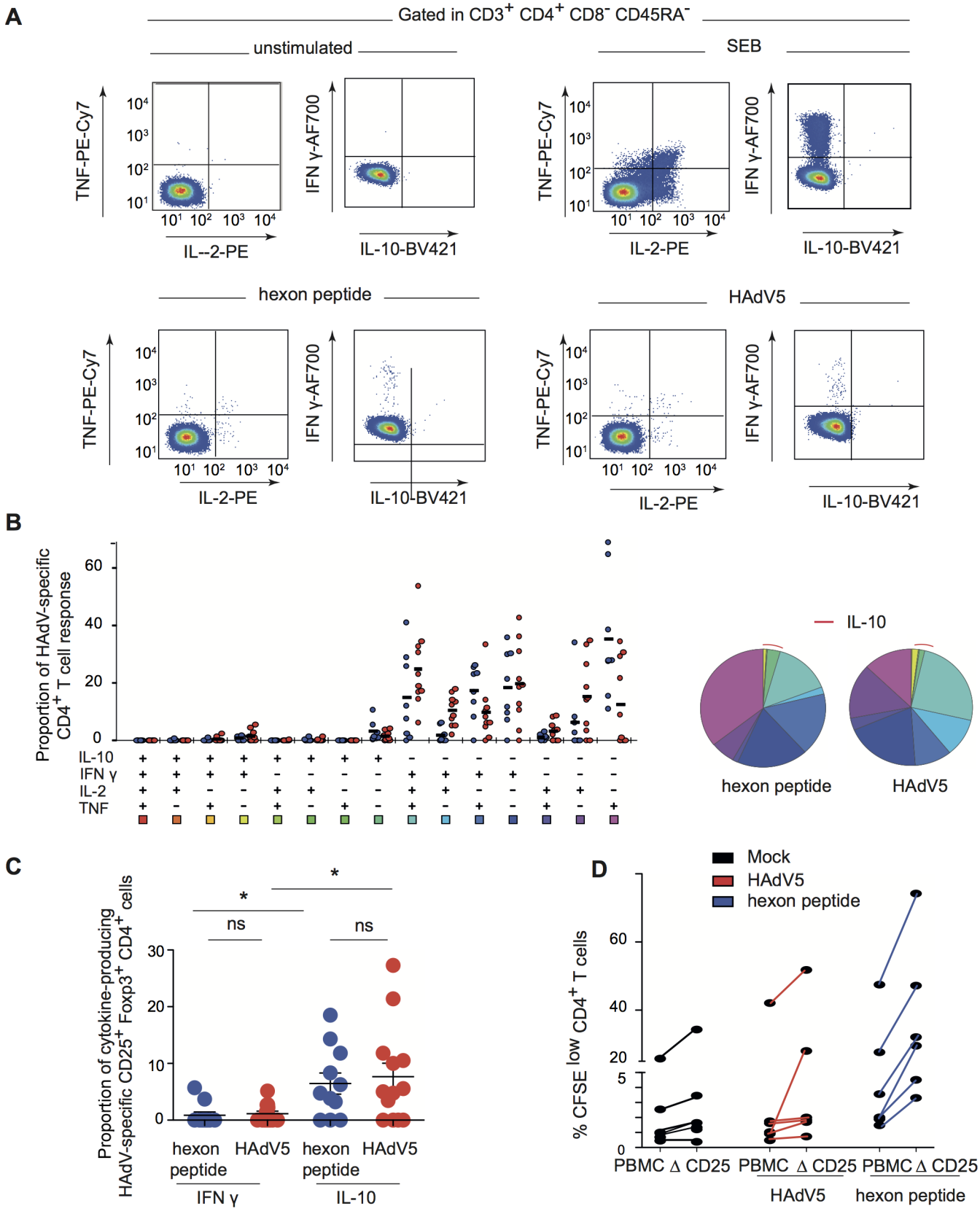
A
Gated in CD3+ CD4+ CD8- CD45RA-
unstimulated
SEB
hexon peptide
HAdV5
TNF-PE-Cy7
IFN γ-AF700
IL--2-PE
IL-2-PE
IL-10-BV421
B
Proportion of HAdV-specific CD4+ T cell response
IL-10
IFN γ
IL-2
TNF
hexon peptide
HAdV5
C
Proportion of cytokine-producing HAdV-specific CD25+ Foxp3+ CD4+ cells
ns
*
hexon peptide
HAdV5
IFN γ
IL-10
D
Mock
HAdV5
hexon peptide
% CFSE low CD4+ T cells
PBMC Δ CD25
HAdV5
hexon peptide

Fig 1. HAdV-specific T_{regs} are present in normal healthy adults. A) Representative flow cytometry profile of hexon peptides- and HAdV5-specific (bottom left and right panels) CD4 T cells producing TNF, IL-2, IFN-γ, and IL-10 in a representative subject. Top left panel: mock stimulated (negative control). Top right panel: cytokine profiles of CD4 T cells stimulated with SEB (Staphylococcal enterotoxin B, positive control). **B**) Cumulative (n = 11 donors) cytokine profiles of hexon peptides (blue points) and HAdV5 (red points) CD4 T cells producing TNF, IL-2, IFN-γ, and IL-10. All possible combinations of responses are shown on the x-axis, and the percentage of functionally distinct cell populations within the CD4 T-cell populations are shown on the y-axis. Responses are grouped and color-coded on the basis of the number of functions. The pie chart summarizes the data, and each slice corresponds to the fraction of CD4 T cells with a given number of functions, within the responding CD4 T cells. Red arcs correspond to IL-10 producing CD4 T cell. **C)** Proportion of IL-10 or IFN-γ-producing HAdV5-specific CD4 T cells expressing CD25 and FoxP3 among IL-10, or IFN-γ, producing HAdV5-specific CD4 T cells. **D)** Proliferation of CFSE-labeled PBMCs and PBMCs depleted in $CD25^+$ cells (ΔCD25) activated by HAdV5 (red lines) or hexon peptides (blue lines) and cultured for 7 days. The cells were analyzed by flow cytometry for proliferation ($CFSE^{low}$) and CD4 using FlowJo software (n = 6 donors and assayed in duplicate).

https://doi.org/10.1371/journal.ppat.1007127.g001

of HAdV-presenting tolerogenic DCs. When HAdV5 is mixed with neutralizing antibodies from human sera, 200 nm-diameter complexes are formed that induce DCs to undergo pyroptosis, or, if the DC does not die, a hypermature profile [13,14]. As these profiles are also inconsistent with that of tolerogenic DCs, we hypothesized that it was not due to IC-HAdV5-activated DCs, but rather an effect on bystander DCs.

To assess the impact of IC-HAdV5-induced pyroptosis and DC maturation on bystander DCs we developed a transwell assay (see **S1A Fig** for schematic). Briefly, $CD14^+$ monocytes isolated from fresh buffy coats were induced to differentiate into immature DCs for 6 days. Immature DCs seeded in 12-well plates were mock-treated, challenged with bacterial lipopolysaccharides (LPS) as a generic control for DC reactivity, HAdV5, IgGs, or IC-HAdV5 (these cells will be referred to "direct DCs"). At 6 h post-challenge, a transwell insert was added and naive immature DCs (bystander DCs) from the same donor were seeded in the upper chamber (see **S1B–S1D Fig** for controls concerning transfer of HAdV5 particles between chambers and cell death). Twelve hours after adding the bystander DCs to the upper chamber, the direct and bystander DCs were collected and assayed as described below. Compared to bystander DCs stimulated by direct DCs challenged with IgG or HAdV5, bystander DCs stimulated by IC-HAdV5-challenged DCs increased their cell surface levels of the maturation/activation markers CD80, CD83, CD86 (**Fig 2A**), CD40, and MHC II (**S2A Fig**). The level of CD86 on bystander DCs tended to increase as the number of IC-HAdV5 particles increased during the stimulation of the direct DCs (**S2B Fig**). The cell surface increase of CD86 and CD83 was also accompanied by an increase in total (cell surface + intracellular) CD86 and CD83 levels (**Fig 2B**). Together, these data demonstrate that IC-HAdV5-challenged DCs enhanced the synthesis and cell surface expression of maturation/activation markers on bystander DCs.

The cytokine transcriptome of bystander DCs suggests a tolerogenic profile

To characterize bystander DC functional capabilities we used an 84-plex inflammatory cytokine, chemokine and their receptor mRNA array to quantify transcriptional changes (see **S2C Fig** for the list of mRNAs that gave unique amplification profiles). Stimulation of bystander DCs with the milieu from HAdV5-challenged DCs (without IgGs) led to notable increases (>50 fold) in mRNA levels of Th1/Th17 cell activation/differentiation markers (e.g. *CXCL9*, *CXC10 & CXC11*) (see **S2C Fig** for all data and **Fig 3A** left hand columns for selected data). By contrast, the bystander DC response to the IC-HAdV5-challenged DCs was greater with respect to the number of mRNAs altered (>20) and magnitude (up to 10,000-fold increase) (**Fig 3A** right column, and **S2C Fig** middle column). Of particular relevance was the lack of *TNF* mRNA by bystander DC because tolerogenic DCs should not, *a priori*, secrete TNF. To better understand the transcriptional responses of the different conditions, we applied a principal component analysis (PCA) to find patterns in these data sets. We found that two principal components (see Materials & Methods for genes in the F1, F2, and F3 axes) explained 89%

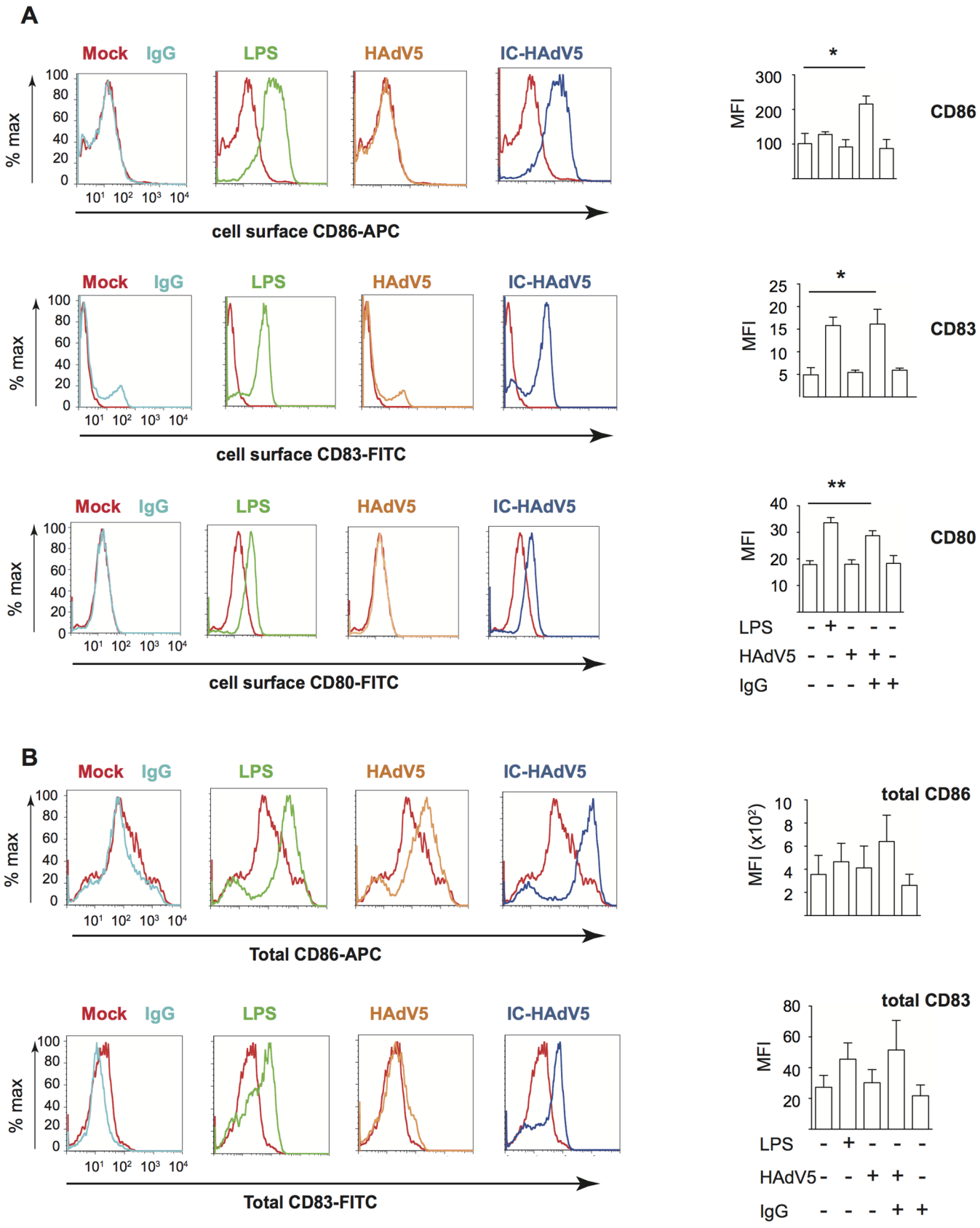
A
Mock
IgG
LPS
HAdV5
IC-HAdV5
% max
cell surface CD86-APC
cell surface CD83-FITC
cell surface CD80-FITC
MFI
CD86
CD83
CD80
LPS
HAdV5
IgG
B
Total CD86-APC
Total CD83-FITC
total CD86
total CD83
MFI (x10²)

Fig 2. Activation/maturation marker expression in bystander DCs. Representative flow cytometry profile and cumulative data of cells that were mock-treated (red), challenged with IgG (light blue), LPS (green), HAdV5 (orange), or IC-HAdV5 (dark blue). **A)** The cell surface expression of CD86 (top panels), CD83 (middle panels), and CD80 (bottom panels) were quantified 12 h post-stimulation. The profile of mock-treated cells is included in each panel as a reference. The graphs to the right are the cumulative data from 5 donors and performed in duplicate. **B)** Representative flow cytometry profile and cumulative data of total (intracellular and extracellular) CD86 and CD83 levels in bystander DCs incubated with DCs challenged with IgG, LPS, HAdV5, or IC-HAdV5 12 h post-stimulation (color-coded as in **A**). The mock-treated cells are included in each panel as references. The graphs to the right are the cumulative data from 4 donors and performed in duplicate. Error bars are ± SEM. * $p < 0.05$, ** $p < 0.01$.

https://doi.org/10.1371/journal.ppat.1007127.g002

and 39% of the total information, respectively, and each stimulus is distinguishable from the others (Fig 3B).

Because a cell infected by one HAdV particle could produce $>10^4$ virions ~36 h later, local and global HAdV levels, as well as IC-HAdV formation, are dynamic at early stages of infection. Of note, IC-HAdV5 causes a dose-dependent induction of pyroptosis in direct DCs [14]. We therefore extended the mRNA array analyses by quantifying dose-dependent response of bystander DCs. Using RT-qPCR we analyzed *TNF*, *IFNβ* and *CXCL10* (Fig 3C) and *IL1β*, *IL12* (p40), *CCL3* and *IL6* (S2D Fig) mRNA levels. In all cases the transcriptional response of bystander DCs varied depending on the IC-HAdV5 challenge dose. These data suggest that the bystander DC response is linked to the percentage of direct DCs undergoing pyroptosis [14].

To characterize time-dependent transcriptional changes in direct DC and bystander DCs, we compared mRNA levels of *TNF*, *IFNβ* (Fig 3D), *Mip-1α* and *IL6* (S3 Fig, which also includes dose-dependent response). Globally, mRNAs that code for pro-inflammatory molecules were 2 to 10-fold greater in direct DCs than in bystander DCs. In addition, only *IL1β* and *Mip1α* mRNA levels changed significantly ($p < 0.01$) over time. These data demonstrate that bystander DCs have a semi-mature transcriptional profile, which is linked to DC pyroptosis, and lack noteworthy levels of *TNF* mRNA [30].

Cytokine secretion by bystander DCs is consistent with a tolerogenic profile

To examine the events downstream the transcriptional response, we quantified the secreted cytokine from direct and bystander DCs. Because proteins can readily diffuse across the transwell membranes, bystander DCs were removed from the upper chamber 12 h post-challenge, rinsed, and then placed in a separate well with fresh medium for 9 h before collecting the medium. The direct DC medium was collected at 12 h post-challenge, or after a wash at 12 h and then collected 9 h later (21 h) to compare conditions similar to that used for bystander DCs (see Fig 4A for schematic). Challenging DCs with HAdV5 alone had a modest effect on their secretome with the exception of a 5- to 10-fold increase in TNFSF10, and CXCL9 & 10 levels (Fig 4B, second column from the left). By contrast, IC-HAdV5-challenged DCs responded with increases of >15 fold in approximately half of the cytokines (Fig 4B, middle columns). These data are consistent with previous results showing the robust maturation of IC-HAdV5-challenged DCs [13,14]. HAdV5-challenge DCs that were rinsed 12 h post-stimulation had overall lower cytokine levels than prior to washing, but TNFSF10, CXCL9, CXCL11, and CCL5 levels remained robust (Fig 4C, middle columns). Interestingly, instead of a positive correlation between the cytokine secretion and the IC-HAdV5 dose, we found that as the IC-HAdV5 dose increased, the cytokines secreted by direct DCs tended to decrease (Fig 4C, middle columns).

Using HAdV5-challenged DCs (without IgGs) to generate bystander DCs, we found that the latter secreted 3- to 12-fold higher levels of TNFSF10, CCL5, CXCL9, CXCL10 and CXCL11 compared to bystander DCs exposed to the medium from IgG-challenged DCs (Fig

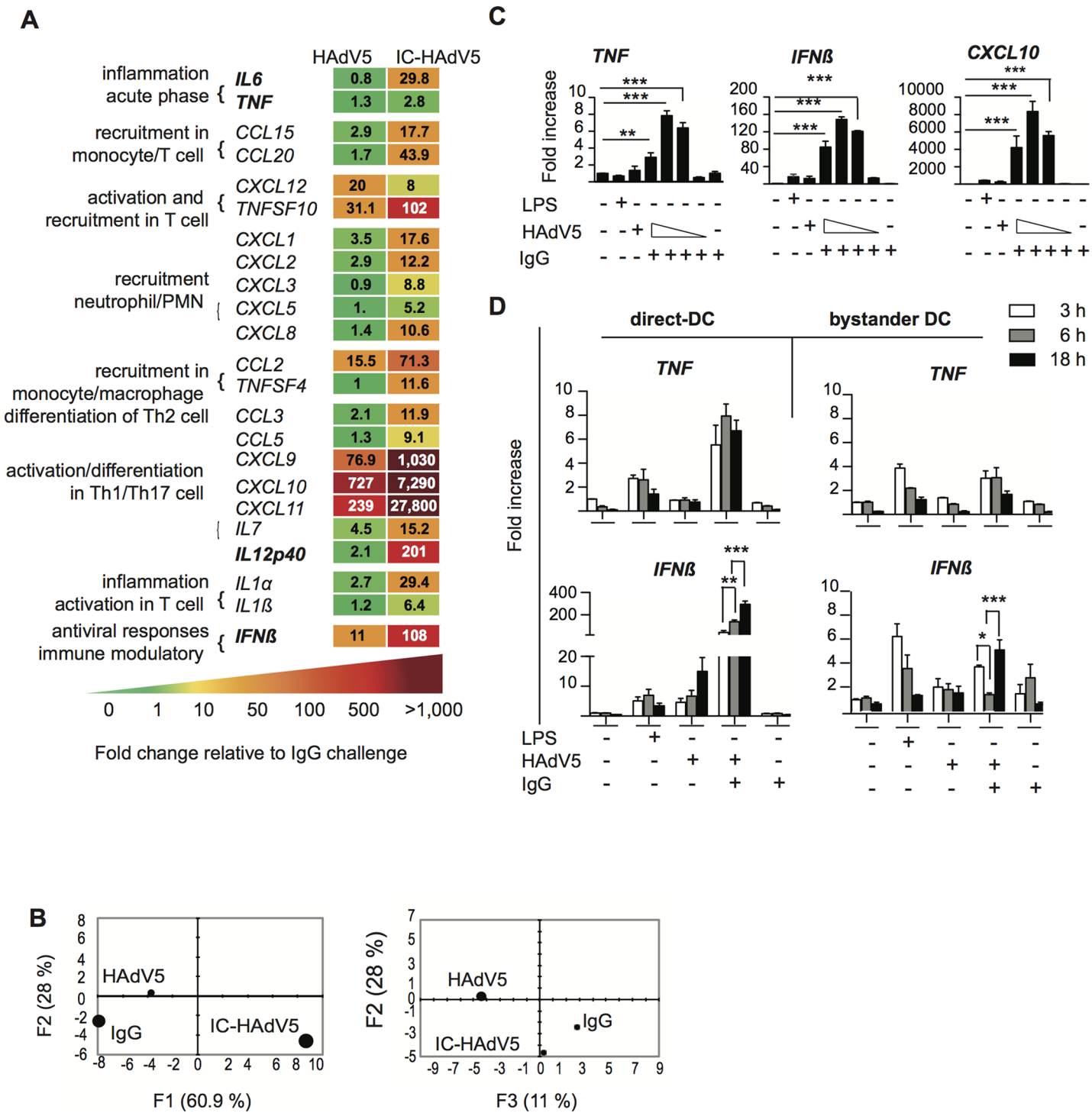

Fig 3. Bystander DC cytokine transcription profile. A) Transcription profile of selected cytokines from bystander DCs at 12 h post-activation following exposure to HAdV5- or IC-HAdV5-challenged direct DCs. The transcription profile of bystander DCs created by IgG-challenged direct DCs was used as the baseline. For the genes in bold, primer sequences were designed in-house (n = 2 donors). **B)** Principal component analysis (PCA) of the changes in the 66 mRNAs included in the array. Three principal components showed 61% (F1), 28% (F2), and 11% (F3) accordance. **C)** *TNF*, *IFNβ*, and *CXCL10* mRNA levels in bystander DCs. Direct DCs were mock-, IgG-, LPS-, HAdV5-, or IC-HAdV5-challenged. IC-HAdV5s were used at 20 x 10^3, 10 x 10^3, 5 x 10^3, or 1 x 10^3 physical particles/direct DC. Assays were carried out in 3 donors in at least duplicates. The fold increase is shown as mean ± SEM. See S1 Table for additional statistical analyses. **D)** Kinetics (3, 6, 18 h) of *TNF (top panels)* and *IFNβ* (bottom panels) mRNA levels of THP-1-derived DC challenged with LPS, HAd5, IgG or IC-HAdV5 (left panels) or bystander DCs (using the milieu from the direct DCs in the left panel) (right panels). Three independent assays in duplicate were performed. The fold increase is shown as the mean ± SEM. *P* values were derived from one-way ANOVA with Dunnett's test: ** $p < 0.01$ and *** $p < 0.001$.

https://doi.org/10.1371/journal.ppat.1007127.g003

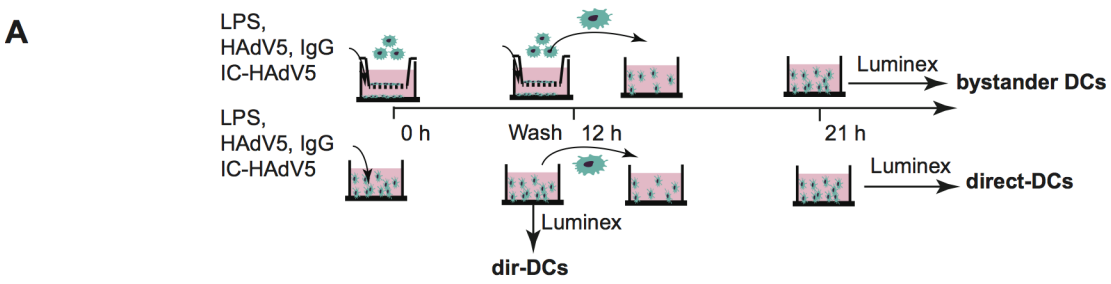

B **direct-DCs** (from 0-12 h)

	IgG	HAdV5	IC-HAdV5			LPS
IL-6	1 (62)	4.3	25.5	46.8	44.6	141
TNF	1 (89)	1.8	44.7	42.3	31.5	61.1
CCL15	1 (379)	1.2	2.2	2.9	3.2	3.6
CCL20	1 (9)	1	25.4	17.4	13.7	110
CXCL12	1 (109)	1.6	2.7	2.9	2.8	4.3
TNFSF10	1 (37)	4.7	6.5	18.6	20.6	6.2
CXCL1	1 (286)	1.6	3.2	2.6	2.3	32.7
CXCL2	1 (100)	1.4	7.5	4.2	2.7	36.0
CXCL5	1 (224)	1.2	3.1	2.5	1.9	6.8
CXCL8	1 (89)	1.8	44.7	42.3	31.5	61.1
CCL2	1 (104)	4.1	4.2	18.1	23.7	6.6
CCL24	1 (7770)	0.8	0.7	0.8	0.9	0.9
CCL3	1 (50)	3.5	40.5	45.1	41.1	46.1
CCL5	1 (86)	1.7	29.7	46.5	41.4	77.2
CXCL9	1 (283)	9.4	15.8	22.4	20.8	34.8
CXCL10	1 (1500)	7.8	6.9	8.9	9.2	7.1
CXCL11	1 (179)	1.8	4.1	6.3	7.0	5.9
IL-7	1 (91)	1.2	2.2	2.2	2.2	1.4
IL-12p40	1 (122)	1	3.4	2.2	2.2	104
IL-1α	1 (4)	1.1	4.0	3.2	2.5	40.7
IL-1ß	1 (1)	1.9	23.4	17.2	11.5	673
IFN-ß	1 (76)	2.0	49.5	58.9	47.1	19.3

C **direct-DCs** (from 12-21 h)

	IgG	HAdV5	IC-HAdV5			LPS
IL-6	1 (1050)	1.7	0.1	0.5	0.7	1.5
TNF	1 (986)	1.8	0.5	1.6	1.9	0.7
CCL15	1 (391)	3.0	0.5	1.2	2.0	1.7
CCL20	1 (115)	1.2	0.3	0.6	0.9	1.8
CXCL12	1 (347)	1.3	0.7	0.9	1.1	1.2
TNFSF10	1 (37)	9.2	2.7	6.9	9.8	3.4
CXCL1	1 (1150)	1.1	0.3	0.4	0.5	1.3
CXCL2	1 (250)	1.6	0.5	0.7	0.8	1.5
CXCL5	1 (571)	1.0	0.5	0.6	0.7	1.4
CXCL8	1 (986)	1.8	0.5	1.6	1.9	0.7
CCL2	1 (325)	2.3	0.1	0.3	0.7	0.1
CCL24	1 (4730)	0.5	0.1	0.1	0.2	0.3
CCL3	1 (308)	5.2	1.8	3.9	4.5	2
CCL5	1 (54)	62.8	27.8	59.0	112	73.5
CXCL9	1 (255)	5.4	4.6	8.8	13	16.2
CXCL10	1 (2370)	5.9	1.2	2.5	3.6	1.9
CXCL11	1 (32)	20.3	4.3	10.2	18.3	7.6
IL-7	1 (91)	1.2	1.1	1.2	1.2	0.8
IL-12p40	1 (208)	1	0.8	0.7	0.7	2.6
IL-1α	1 (11)	1.8	0.6	0.6	0.5	14.7
IL-1ß	1 (36)	2.3	0.1	0.1	0.2	2.4
IFN-ß	1 (73)	2.2	7.1	12.8	13.9	1.1

D **bystander DCs** (from 12-21 h)

		IgG	HAdV5	IC-HAdV5			LPS
inflammation acute phase	IL-6	1 (238)	1.4	0.7	1.5	1.1	6.5
	TNF	1 (160)	1.3	1.3	1.8	1.1	4.5
recruitment in monocyte/T cell	CCL15	1 (205)	2.8	6.4	7.3	7.6	3.2
	CCL20	1 (22)	1.5	3.3	4.2	2.1	9.7
activation and recruitment in T cell	CXCL12	1 (190)	1.5	2.5	2.4	2.3	2.3
	TNFSF10	1 (25)	6.0	11.1	11.1	9.8	5.1
recruitment neutrophil/PMN	CXCL1	1 (277)	1.5	1.8	1.8	1.7	5.5
	CXCL2	1 (89)	1.6	1.9	1.9	1.6	4.1
	CXCL5	1 (261)	1	1.2	1.4	1.2	3.1
	CXCL8	1 (160)	1.3	1.3	1.8	1.1	4.5
recruitment in monocyte/macrophage differentiation of Th2 cell	CCL2	1 (90)	4.3	4.6	5.4	5.4	0.5
	CCL24	1 (4130)	0.7	0.5	0.5	0.6	0.3
activation/differentiation in Th1/Th17 cell	CCL3	1 (63)	1.3	2.1	3.0	1.7	9.5
	CCL5	1 (32)	2.9	42.5	41.8	17.7	126
	CXCL9	1 (234)	4.8	37.2	32.2	18.6	17.7
	CXCL10	1 (2230)	5.1	4.7	4.6	4.7	2.0
	CXCL11	1 (39)	11.8	28.2	26.2	25.8	6.3
	IL-7	1 (60)	1	1.1	1.1	1.0	1.2
	IL-12p40	1 (87)	0.9	1.1	1.1	0.9	6.2
inflammation activation in T cell	IL-1α	1 (3)	1.1	1	2.2	1.1	57.2
	IL-1ß	1 (2)	1.6	2	2.8	1.3	41.3
antiviral responses immune modulatory	IFN-ß	1 (74)	1.0	1.1	1.1	1.1	1.1

0 1 10 50 100 >500

Fig 4. Direct and bystander DC cytokine secretomes. A) Schema showing how DCs were activated with LPS, HAdV5, IgG, and IC-HAdV5 and when the cell supernatants were harvested. **B)** Cytokine secretion from IgG-, HAdV5-, dose-dependent IC-HAdV5-, and LPS-challenged DCs at 12 h. **C)** Cytokine secretion from IgG-, HAdV5-, dose-dependent IC-HAdV5-, and LPS-challenged DCs at 12–21 h. **D)** Cytokine secretion from bystander DCs (the stimulus used to challenge the direct DCs is above each column at 12–21 h). The color code shows relative increases compared to IgG-challenged-DCs (raw values in first column). The assays were performed twice in duplicate with similar results.

https://doi.org/10.1371/journal.ppat.1007127.g004

4D, second column). Similarly, when bystander DCs were generated using IC-HAdV5-challenged DCs, the level of the above five cytokines also increased. In addition, three chemokines involved in immune cell recruitment (CCL15, CCL20, and CCL2) increased >3 fold. Consistent with the transcriptome analyses, we did not find a notable dose-dependent effect on bystander DCs when direct DCs were incubated with increasing IC-HAdV5 particles (Fig 4D, middle columns).

Together, these data suggest that the release of pathogen-associated molecular patterns (PAMPs), danger-associated molecular patterns (DAMPs), and/or the increased levels of cytokines secreted by a greater number of DCs that do not undergo pyroptosis, are key factors in bystander DC maturation. In addition, the environment created by IC-HAdV5 induces a semi-mature cytokine secretion profile in bystander DCs.

Cytokines and pyroptosis-associated factors impact bystander DC phenotype

To determine how cytokines and pyroptosis impact bystander DCs, we used a combination of drugs and mutant HAdVs to selectively modify the environment created by IC-HAdV5-challenged DCs. To determine the impact of IL-1β, direct DCs were pre-treated with ZVAD, a pan-caspase inhibitor that blocks caspase 1 auto-cleavage and pro-IL-1β processing. Importantly, ZVAD has no effect on TNF and canonical protein secretion (S4A Fig and reference [14]). We found that blocking IL-1β production by direct DCs reduced bystander DC maturation as demonstrated by their lower levels of CD86 and CD83 (Fig 5A and 5B). We then used brefeldin A to block ER to Golgi-mediated cytokine secretion in direct DCs (see S4B Fig for controls). Of note IL-1β release is not significantly affected by brefeldin A, (S4C Fig). In brefeldin A-treated IC-HAdV5-challenged DCs the levels of CD83 and CD86 did not change markedly (Fig 5C), while the bystander DCs responded with lower levels of CD83 and CD86 (Fig 5D).

Next, we generated ICs using Ad^{L40Q} [31], an HAdV5 capsid containing a mutated protein VI that attenuates endosomolysis. While IC-Ad^{L40Q} poorly induces pyroptosis in direct DCs [14], they secrete levels of TNF that are similar to IC-HAdV5-challenged DCs. Furthermore, *IFNβ* and *IL1β* mRNA levels are lower [14]. We found notably lower levels of CD86 and CD83 on bystander DCs following stimulation with the response from IC-HAdV5 versus IC-Ad^{L40Q}-challenged DCs. In addition, the reduced maturation/activation effects were only modestly altered by increasing the IC-Ad^{L40Q} dose (Fig 5E). Together, these data demonstrate a role for pyroptosis-associated factors in the maturation of bystander DCs.

We then compared cytokine mRNA levels in bystander DCs stimulated by HAdV5-, IC-Ad^{L40Q}-, or IC-HAdV5-challenged DCs (Fig 5F and S5A–S5C Fig). Consistent with the phenotype, the transcriptional responses of bystander DCs to both ICs were globally higher than to HAdV5 alone. The bystander DC transcriptional response to IC-Ad^{L40Q}-challenged DC milieu was generally lower than in IC-HAdV5-challenged DCs, and it was qualitatively distinguishable as determined by PCA (Fig 5G).

We then assessed the effect of pyroptosis using IC-Ad2ts1. Ad2ts1 has a hyper-stable capsid due to a mutation in protease that results in failure to process the capsid pre-protein [32,33].

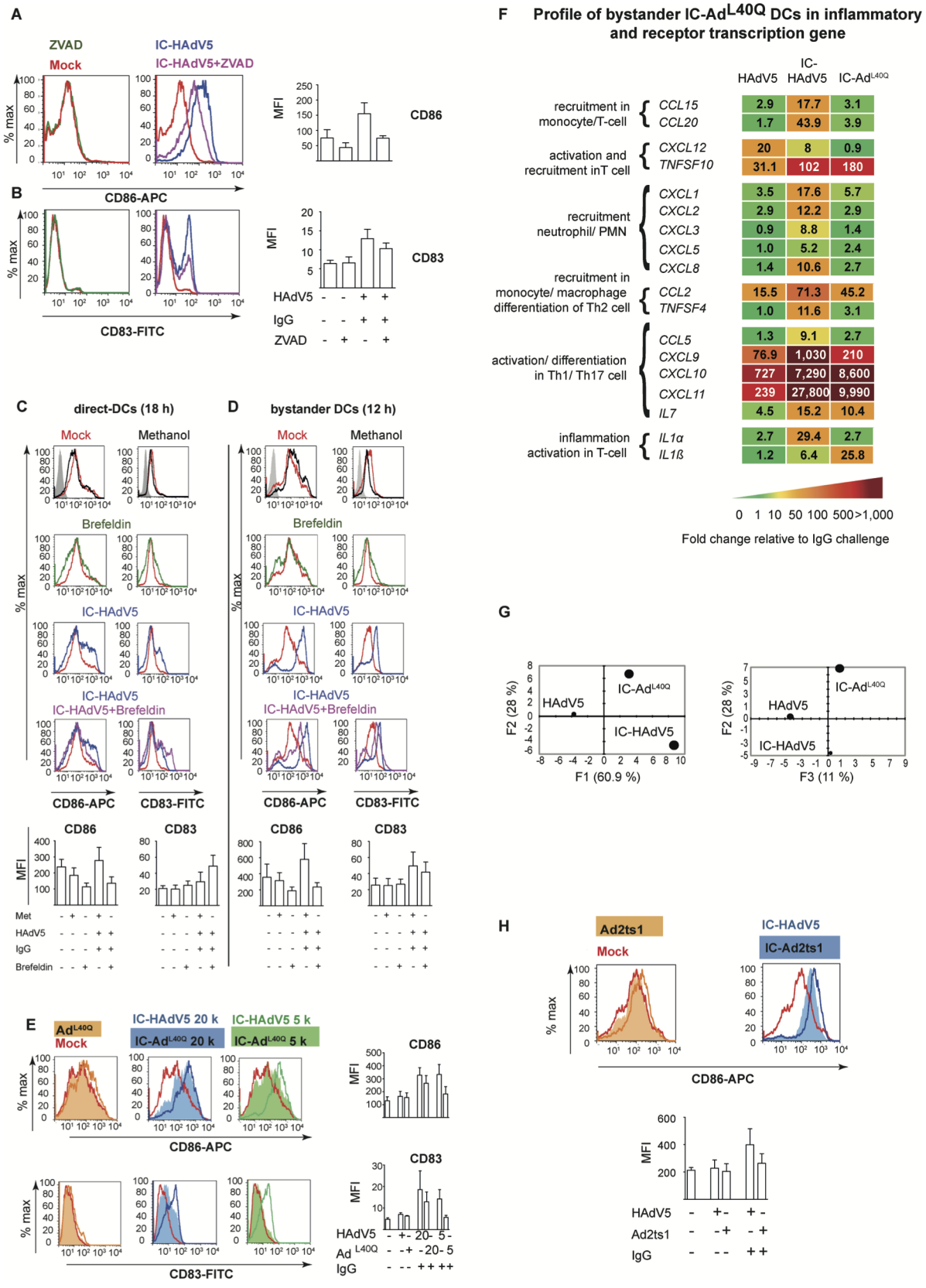
A
ZVAD
Mock
IC-HAdV5
IC-HAdV5+ZVAD
% max
CD86-APC
MFI
CD86
B
CD83-FITC
CD83
HAdV5
IgG
ZVAD
C
direct-DCs (18 h)
D
bystander DCs (12 h)
Methanol
Brefeldin
IC-HAdV5+Brefeldin
Met
Brefeldin
E
Ad^L40Q
IC-HAdV5 20 k
IC-HAdV5 5 k
IC-Ad^L40Q 20 k
IC-Ad^L40Q 5 k
F
Profile of bystander IC-Ad^L40Q DCs in inflammatory and receptor transcription gene
IC-HAdV5
IC-Ad^L40Q
recruitment in monocyte/T-cell
CCL15
CCL20
2.9
17.7
3.1
1.7
43.9
3.9
activation and recruitment inT cell
CXCL12
TNFSF10
20
8
0.9
31.1
102
180
recruitment neutrophil/ PMN
CXCL1
CXCL2
CXCL3
CXCL5
CXCL8
3.5
17.6
5.7
2.9
12.2
2.9
0.9
8.8
1.4
1.0
5.2
2.4
1.4
10.6
2.7
recruitment in monocyte/ macrophage differentiation of Th2 cell
CCL2
TNFSF4
15.5
71.3
45.2
1.0
11.6
3.1
activation/ differentiation in Th1/ Th17 cell
CCL5
CXCL9
CXCL10
CXCL11
IL7
1.3
9.1
2.7
76.9
1,030
210
727
7,290
8,600
239
27,800
9,990
4.5
15.2
10.4
inflammation activation in T-cell
IL1α
IL1ß
2.7
29.4
2.7
1.2
6.4
25.8
0 1 10 50 100 500>1,000
Fold change relative to IgG challenge
G
F2 (28 %)
F1 (60.9 %)
F3 (11 %)
HAdV5
IC-Ad^L40Q
IC-HAdV5
H
Ad2ts1
Mock
IC-HAdV5
IC-Ad2ts1
CD86-APC
HAdV5
Ad2ts1
IgG

Fig 5. Impact of cytokines and pyroptosis-associated factors on bystander DC maturation. A & B) Shown are representative flow cytometry profile and cumulative data of direct DCs pretreated with ZVAD using the approach described in S1 Fig. The cell surface levels of CD86 and CD83 on bystander DCs was quantified by flow cytometry (n = 3 donors). **C & D)** Representative flow cytometry profile and cumulative data of IC-HAdV5-challenged DCs treated with brefeldin A and the cell surface and intracellular levels of CD86 and CD83 quantified by flow cytometry in direct DCs and bystander DCs (n = 5 donors). **E)** Bystander DCs were incubated with milieu generated by DC challenged with increasing doses of IC-Ad^{L40Q} (representative flow cytometry profiles and cumulative data of CD86 and CD83 levels) (n = 3 donors). **F)** Bystander DC inflammatory cytokine mRNA levels were measured by RT-qPCR array following incubation with DC challenged with HAdV5, IC-HAdV5 and IC-Ad^{L40Q}. The heat map denotes the fold change relative to DCs challenged by IgGs (n = 3 donors). **G)** PCA of the changes in the 66 mRNAs included in the array when including IC-Ad^{L40Q}. **H)** Bystander DCs were incubated with milieu generated by DCs challenged with increasing doses of IC-Ad2ts1. Representative flow cytometry profiles and cumulative data of cell surface level of CD86 (n = 2 donors).

https://doi.org/10.1371/journal.ppat.1007127.g005

We previously showed that IC-Ad2ts1 poorly induces DC pyroptosis, likely because the HAdV genome does not escape from the capsid and therefore does not nucleate AIM2 (see reference [14] and S5D–S5F Fig for Ad2ts1 controls). Of note, TNF levels are comparable in DCs challenged with IC-Ad2ts1 or IC-HAdV5 [14]. Here, we found that IC-Ad2ts1-challenged DC induced an increase of CD86 cell surface levels on bystander DCs (Fig 5H**).** Together, these data demonstrate that cytokines, DAMP, and PAMPs play a role in the activation and semi-maturation of bystander DCs.

Engagement of TLR4 on bystander DCs

To characterize how bystander DCs are activated, we focused on Toll-like receptor 4 (TLR4). TLR4 is a multi-functional cell surface PRR that can directly or indirectly (by forming a complex with MD-2, CD14, or other PRRs) be activated by extracellular viral components (PAMPs) and, under inflammatory conditions, extracellular high-mobility group box 1 and heat shock proteins (DAMPs) [34–36]. Of note, MD-2 acts as a co-receptor for recognition of both exogenous and endogenous ligands [37–40]. While TLR4 does not bind to, or become activated by, HAdV5 alone [41], TLR4 might be activated by PAMPs or DAMPs that interact directly with the HAdV5 capsid. We therefore used TAK-242 to disrupt TLR4 signaling in bystander DCs (see S6 Fig for TAK-242 control). As readouts, we used the upregulation of *TNF* and *IL1β* mRNAs, and activation/maturation cell surface markers. When TLR4 signaling was blocked in bystander DCs stimulated by the IC-HAdV5-challenged DC milieu, there was a significant ($p < 0.05$) decrease in *IL1β* mRNA levels and 2-fold decrease of *TNF* mRNA (Fig 6A). CD83 and, to a lesser extent, CD86 levels were also reduced (Fig 6B). These data suggest that bystander DCs use TLR4 to detect PAMPs and DAMPs released by IC-HAdV5-challenged DCs, leading to changes in bystander DC maturation.

Minimal loss of phagocytosis in bystander DCs is consistent with tolerogenic profile

Immature DCs survey the extracellular environment by random phagocytosis. Once PRRs are engaged, DC maturation is accompanied by decreased uptake of fluid phase molecules [42]. Of note, a functional hallmark of tolerogenic DCs is their ability to retain some antigen uptake properties. To address the functional maturation of IC-HAdV5-challenged DCs and bystander DCs, we incubated cells with FITC-labeled dextran and quantified uptake by flow cytometry. We found that phagocytosis was modestly decreased in direct DCs stimulated with HAdV5 or LPS (Fig 7A). By contrast, IC-HAdV5-challenged DC phagocytosis was near background levels, consistent with complete maturation (see S7 Fig for controls) [29]. While bystander DCs had reduced phagocytosis when created by IC-HAdV5-challenged DCs, the bystander DCs still took up 17-fold more FITC-dextran than background levels (Fig 7B). These functional data are consistent with semi-mature, tolerogenic DC profile.

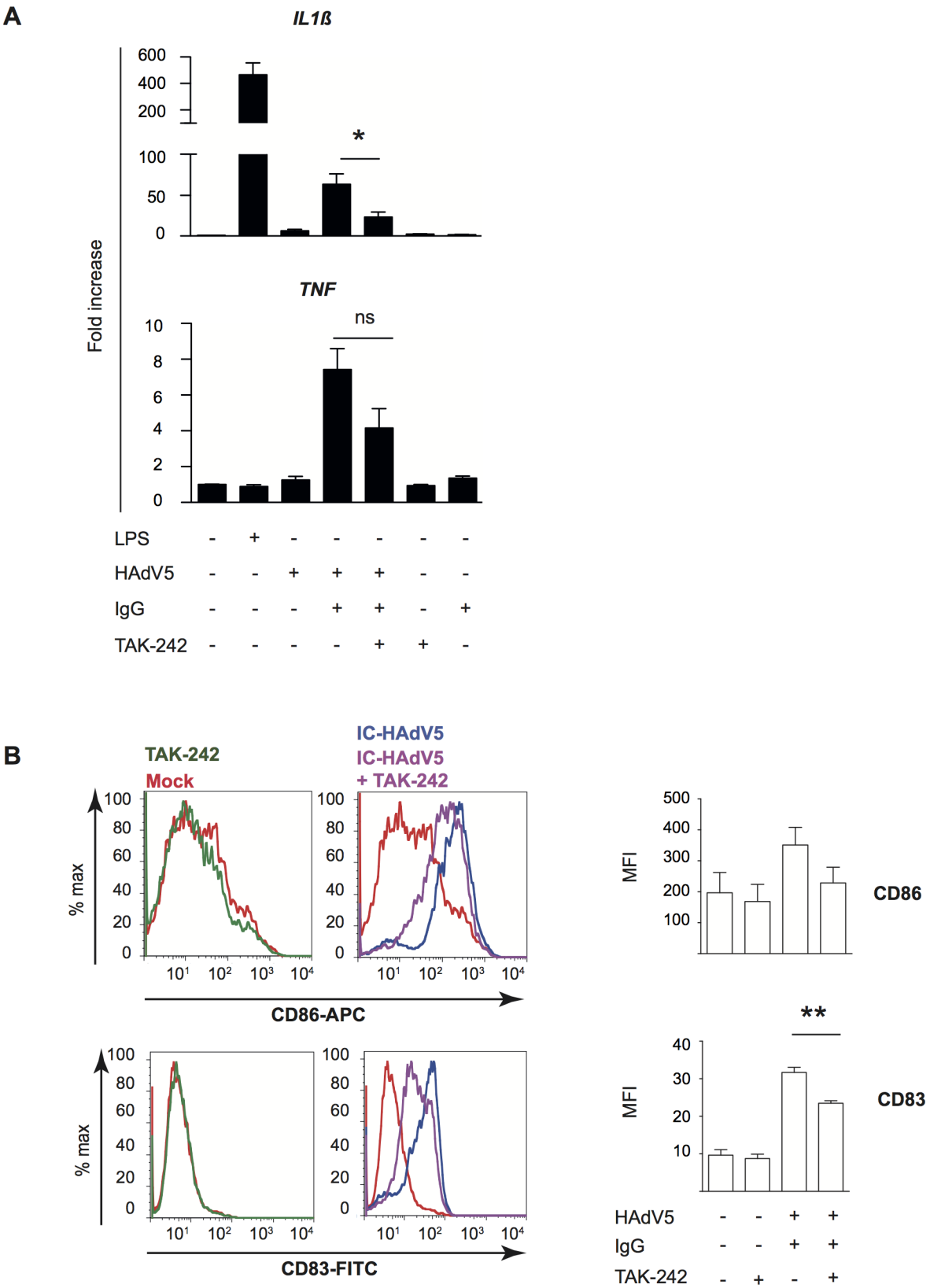

Fig 6. Impact of TLR4 engagement on cytokine transcription and activation and maturation markers in bystander DCs. Involvement of TLR4 signaling in bystander DCs was assessed by **A)** *IL1β* and *TNF* mRNA levels in bystander DCs pre-treated with TAK-242, and then

added to milieu of DCs challenged with LPS, IgG, HAdV5 and IC-HAdV5. Fold increase is represented as mean ± SEM (n = 3 donors, * denotes $p < 0.05$) **B)** Representative flow cytometry profiles and cumulative data of CD86 and CD83 cell surface levels in bystander DCs. DCs were mock-treated (red line), TAK-242 alone (with TAK-242 and without direct DCs, green line) challenged with IC-HAdV5 (dark blue) or pretreated with TAK-242 and challenged with the milieu generated from IC-HAdV5-challenged DCs (violet line) (n = 3 donors, ** denotes $p < 0.001$).

https://doi.org/10.1371/journal.ppat.1007127.g006

Bystander DCs recruit monocytes

While tolerogenic DCs can induce, recruit, and maintain T_{reg} homeostasis, tolerogenic DCs can also create a feedback loop to promote their own generation [43]. Because monocytes are recruited to sites of inflammation [44,45], we compared the recruitment capabilities of direct DCs and bystander DCs (see **S8 Fig** for setup and controls). Unexpectedly, we found that IC-HAdV5-challenged DCs inhibited monocyte recruitment in an IC-HAdV5 dose-dependent manner (**Fig 8A & 8B**). Of note, the inhibition was abrogated when the IC-HAdV5-challenged DCs were washed, suggesting that inhibitory factors were generated <3 h post-IC-HAdV5 challenge (**Fig 8B**). To determine if pyroptosis-related factors (i.e. IL-1β, DAMPs and PAMPs) are responsible for the inhibition of monocyte recruitment, we used ZVAD and IC-Ad^{L40Q} to reduce pyroptosis. ZVAD, which prevents caspase 1 auto-activation, IL-1β maturation, and GSDMD-associated pore formation, modestly increased monocyte recruitment induced by IC-HAdV5-challenged DC (**Fig 8C & 8D**). In contrast to the IC-HAdV5-challenged DC response, the IC-Ad^{L40Q}-challenged DC response significantly ($p < 0.05$) increased monocyte recruitment, in a dose-dependent manner (**Fig 8E & 8F**). These data suggest that DC pyroptosis inhibits monocyte recruitment.

We then examined the ability of bystander DCs to recruit monocytes. In contrast to IC-HAdV5-challenged DCs, bystander DCs promoted monocyte recruitment (**Fig 8G**). These data are consistent with the bystander DC milieu containing more chemoattractants (**Fig 5**). There was also a trend towards greater recruitment when higher IC-HAdV5 doses were used to stimulate the direct DCs.

Once monocytes migrate into an inflammatory environment they acquire distinct phenotypic and functional profiles [46]. One phenotypic hallmark of monocyte differentiation is CD14, which is high on monocytes and macrophages, but lower on DCs. We therefore characterized migrating and static monocytes for CD14 and CD86 levels at 24 and 72 h (see schematic at the left of each panel in **Fig 8H–8J** for the times and location of cells, and **S8 Fig** for controls). At 24 h the level of CD14 on monocytes that had migrated into the bystander DCs environment did not change markedly, while CD86 levels were lower (**Fig 8H**). At 72 h the recruited monocytes had two distinct populations based on CD14 levels (**Fig 8I**). The decrease in CD14 levels suggested that they differentiated into DCs, while the CD86 levels suggest the maintenance of an immature phenotype. In addition, monocytes recruited by bystander DCs had increased CD14 levels. By contrast, CD86 levels decreased on monocytes in the upper chamber (bottom chamber containing bystander DCs) (**Fig 8J**).

Together, these data demonstrate that DCs challenged with IC-HAdV5 inhibit monocyte recruitment. Monocytes recruited to the bystander DC environment was abetted by pyroptosis of the direct DCs. Recruited monocytes had reduced CD14 levels, possibly due the engagement and internalization of TLR4/CD14 complexes. Monocyte-DC contact also appeared to favor the increase in cell surface levels of activation/maturation markers. We concluded that the dynamic environment created by bystander DCs is consistent with a feed-forward loop to foster tolerogenic DCs.

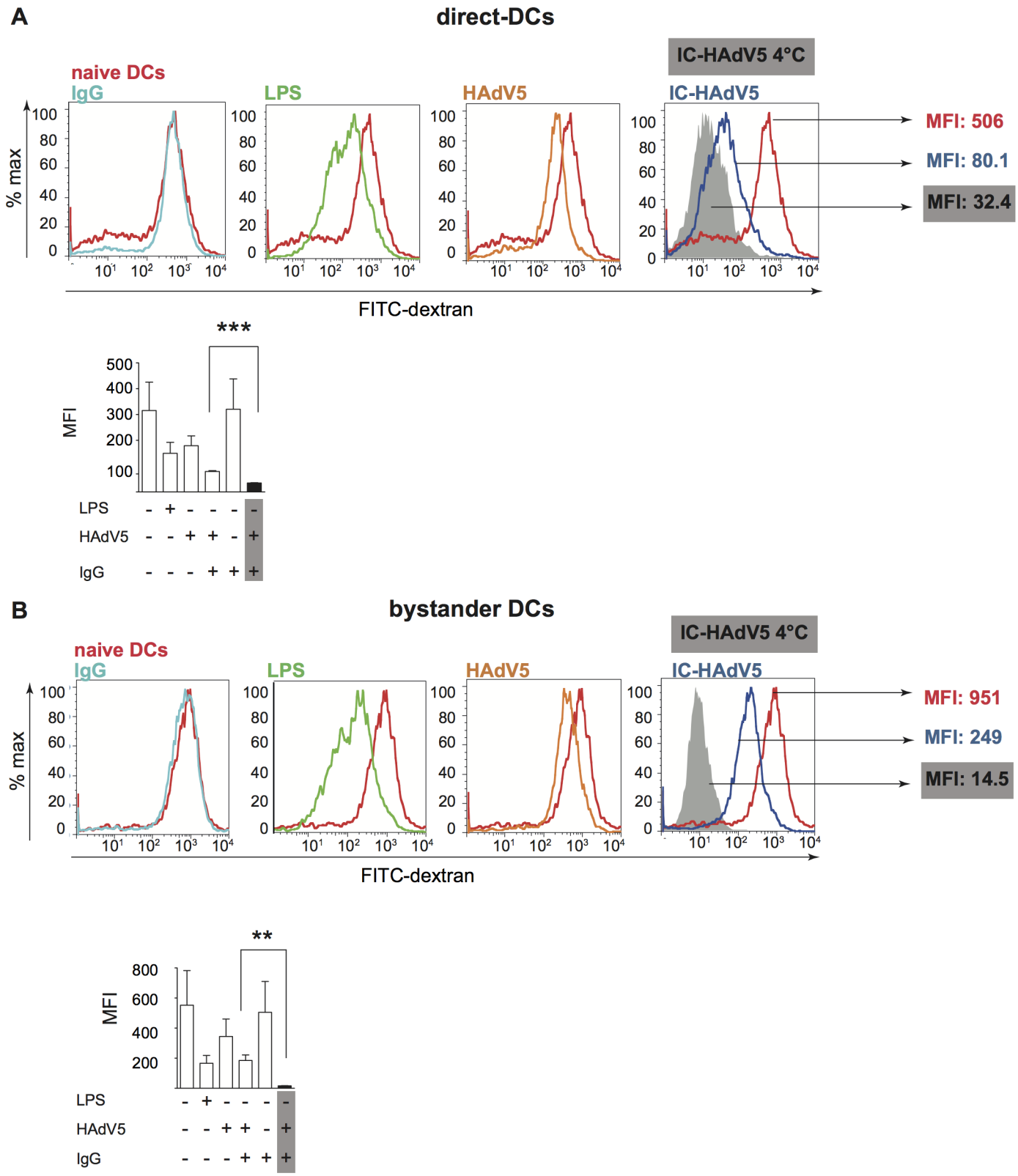

Fig 7. Fluid phase uptake by direct and bystander DCs. Fluid phase antigen uptake by direct and bystander DCs was quantified using FITC-labeled dextran and flow cytometry. **A)** Representative flow cytometry profiles and cumulative data of direct DCs challenged with LPS, HAdV5, IgG, or IC-HAdV5 and **B)** Representative flow cytometry profiles and cumulative data of bystander DCs with the corresponding direct DC milieu. Nonspecific binding of dextran to cells was controlled by incubation at 4˚C (S7 Fig). MFI–median fluorescent index; n = 3 donors, in duplicate.

https://doi.org/10.1371/journal.ppat.1007127.g007

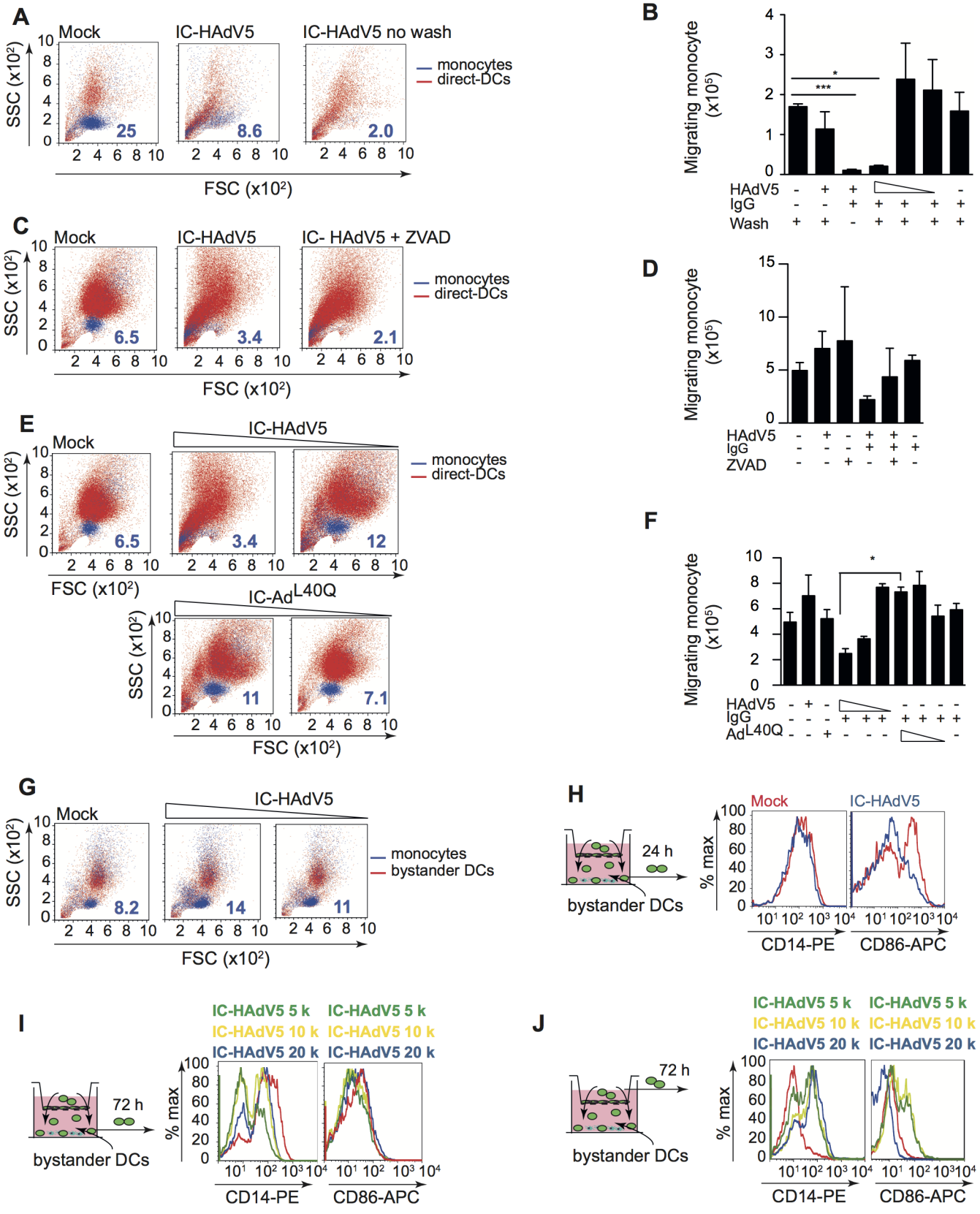
A
Mock
IC-HAdV5
IC-HAdV5 no wash
SSC (x10²)
FSC (x10²)
25
8.6
2.0
monocytes
direct-DCs
B
Migrating monocyte (x10⁵)
HAdV5
IgG
Wash
C
Mock
IC-HAdV5
IC- HAdV5 + ZVAD
6.5
3.4
2.1
D
ZVAD
E
IC-HAdV5
IC-Ad^L40Q
12
11
7.1
F
G
8.2
14
11
bystander DCs
H
24 h
% max
CD14-PE
CD86-APC
I
72 h
IC-HAdV5 5 k
IC-HAdV5 10 k
IC-HAdV5 20 k
J

Fig 8. Direct and bystander DC monocyte recruitment and their phenotype. A 5 μm-pore transwell system (see S8 Fig for details) was used for monocyte migration assays. **A)** Representative FSC/SSC profiles of CFSE-labeled monocyte (blue) that migrated into the lower direct DC chamber; The numbers in dark blue correspond to the percentage of CFSE-labeled monocytes. **B)** Cumulative data from monocyte migration at 24 h into the lower chamber containing DCs challenged with HAdV5, IgGs or decreasing doses (20 x 10^3, 10 x 10^3 and 5 x10^3) of IC-HAdV5 and washed after 30 min post-challenge; data are mean ± SEM, n = 4 donors; **C)** Representative FSC/SSC profiles of direct DCs (red) pretreated with ZVAD before activation with IC-HAdV5. The CFSE-stained monocytes (blue) were added to the upper compartment and migration was quantified at 24 h; Numbers in dark blue correspond to the percentage of CFSE-labeled monocytes. **D)** Cumulative data from assay in (**C**) n ≥3 donors; **E)** Representative FSC/SSC profiles of DCs (red) challenged with decreasing doses of IC-HAdV5 or IC- Ad^{L40Q} and CFSE-labeled monocyte (blue) recruitment at 24 h. The numbers in dark blue correspond to the percentage of CFSE-labeled monocytes. **F)** Cumulative data from assay in (**E**) using DCs from ≥3 donors; **G)** Bystander DCs activated for 12 h with milieu from DC challenged with increasing concentration of IC-HAdV5. The bystander DCs were seeded in the lower chamber of a transwell and CFSE-labeled monocyte recruitment was quantified by flow cytometry at 24 h (n ≥4 donors). The numbers in dark blue correspond to the percentage of CFSE-labeled monocytes. **H)** Phenotypic characterization of the monocytes (green cells seeded in the upper chamber) recruited by bystander DCs. DCs were challenged with increasing doses of IC-HAdV5 (colored coded on top of each panel). The milieu from these direct DCs was used to generate bystander DCs. The bystander DCs were seeded in the lower chamber of the transwell system and the monocytes that were recruited were characterized for their expression of CD14 and CD86 at 24 h, and **I)** at 72 h. **J)** Monocytes that did not migrate into the lower chamber were also characterized for the CD14 and CD86 levels. The data are representative flow cytometry profiles of experiments carried out in ≥5 donors. *p* values in **B, D,** and **F** were derived from *t*-tests: * $p < 0.05$, ** $p < 0.01$, and *** $p < 0.001$.

https://doi.org/10.1371/journal.ppat.1007127.g008

Bystander DCs induce memory T-cell proliferation and naïve CD4 T cells towards HAdV-specific T_{regs}

A functional characteristic of tolerogenic DCs is that they can take up and present antigens. Therefore, we asked if some of the bystander DCs generated in our ex vivo model are capable of inducing proliferation of HAdV5-specific memory T cells. We used IC-HAdV-challenged DC to generate bystander DCs, which were then added to CFSE-labeled PBMCs. Seven days post-incubation we found that $CD3^+/CFSE^{low}$ cells harbored memory T cell markers ($CD45RO^+/CD45RA^-$) (Fig 9A). These data are consistent with the potential of some of the bystander DCs to maintain fluid phase uptake and subsequent presentation of HAdV5 antigens to memory T cells.

In addition to antigen presentation, tolerogenic DCs can induce naïve $CD4^+$ cells to become T_{regs}. To address this functional characteristic, bystander DCs were generated and incubated with autologous naïve $CD4^+/CD45RA^{high}$ cells for 3 or 7 days. The T cells were then assayed by multi-parametric flow cytometry for CD4, CD25, CD127 and FoxP3, markers that are indicative of T_{regs}. While activated T cells transiently express FoxP3 (S9 Fig), the relatively low-level does not result in acquisition of suppressor activity [27]. By contrast, stable and high levels of FoxP3 can be used to identify *bona fide* T_{regs}. At day 3, naïve T cells expressed T_{reg} markers in all conditions (except mock-treated direct DCs) (Fig 9B). At day 7, the number cells with T_{reg} phenotype was near background following incubation in the milieu of mock-, IgG-, or HAdV5-challenged direct DC (Fig 9C). By contrast, bystander DC created from IC-HAdV-direct DCs had a significant ($p < 0.05$) increase in cells with a T_{reg} profile. These data demonstrate that bystander DCs can induce naïve CD4 into cells with a T_{reg} phenotype, further supporting our conclusion that they are tolerogenic DCs.

As shown in Fig 1D, healthy adults harbor $CD25^+$ cells can inhibit HAdV-specific $CD4^+$ cell proliferation. We therefore asked if the tolerogenic bystander DCs generated in our ex vivo assay could induce the production of HAdV-specific T_{regs}. To address this question we isolated PBMCs, $CD14^+$ monocytes, and naïve $CD4^+$ T cells from 3 donors that harbored anti-HAdV memory T cells (see S10 Fig for flow chart). Briefly, monocytes were used to create direct DCs that were incubated with IC-HAdV-C5. Bystander DCs were generated as previously described. VPD 450-labeled naïve $CD4^+$ T cells were incubated with bystander DCs to generate T_{regs}. VPD $450^{low}/CD4^+/CD25^+$ cells (600 to 5,000 cells) were isolated by FACS and mixed with CFSE-labeled PBMCs ± hexon peptides. We found that the ex vivo generated T_{regs} from 3/3 donors reduced the proliferation of anti-HAdV T cells ($CFSE^{low}/CD4^+$) (Fig 9D). These data demonstrate that HAdV-specific T_{regs} can be generated via bystander DCs.

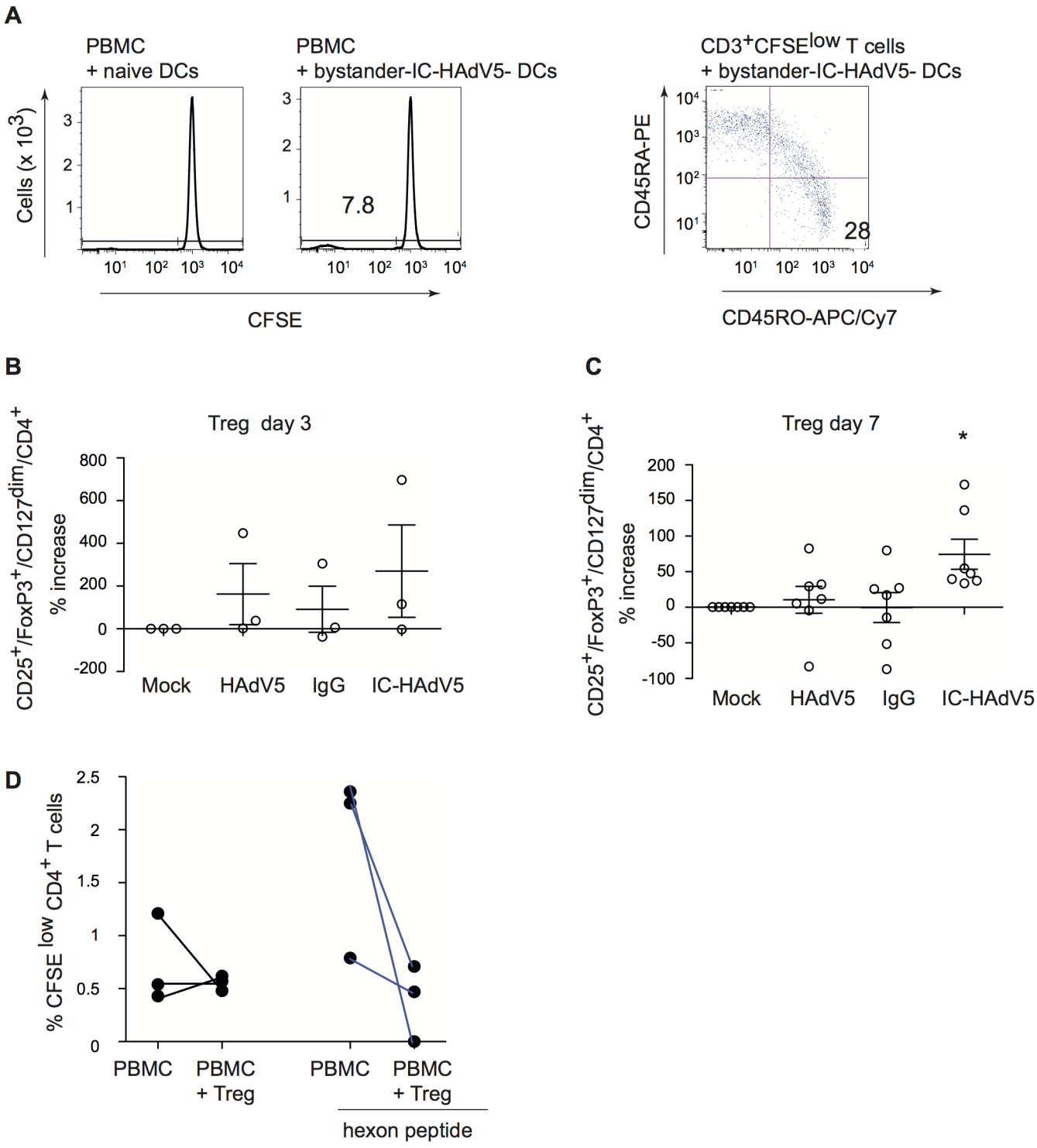

Fig 9. Bystander DCs induce memory T cell proliferation and promote naïve CD4 cells towards T_{reg} phenotype that inhibit proliferation of anti-HAdV T cells. A) Bystander DCs, generated via IC-HAdV stimulation of direct DCs or mock-treated DCs, were incubated with CFSE-labeled PBMCs and proliferation was quantified by flow cytometry. $CD3^+/CFSE^{low}$ cells were screened for memory T cell profile (CD45RO vs. CD45RA). Bystander DCs, generated using the media from DCs challenged with IgG, HAdV5, and IC-HAdV5, were incubated with 10^5 naive $CD4^+$ T (ratio of 10:1 PBMC/ bystander DC) cells isolated from the same donors. The percentage of T_{regs} ($CD25^+/FoxP3^{high}/CD127^{dim}/CD4^+$ cells) varies between 1 to 5% of $CD4^+$ cells in peripheral blood. The number of T_{regs} in the $CD4^+$ cell population, ± bystander DCs, was quantified by analyzing 50,000 cells by flow cytometry. The results are presented as percentage of increase of mock-treated cells at day 3 (**B**) or day 7 (**C**). **D)** T_{regs} generated by bystander DCs reduce the proliferation of memory anti-HAdV CD4 T cells. Experiments were carried out in ≥7 donors with similar results. * $p < 0.05$ vs. mock, HAdV5 and IgG.

https://doi.org/10.1371/journal.ppat.1007127.g009

Discussion

HAdV infections lead to multifaceted, robust, long-lived cellular and humoral responses in most young immunocompetent adults. Nonetheless, several HAdV types somehow circumvent immune surveillance to establish persistent infections. It is well documented that HAdV neutralizing antibodies are type specific, while the anti-HAdV cellular response is cross-reactive [1,3,8,47–49]. In addition, it is the anti-HAdV cellular response that protects us from reactivation of persistent infections. The dichotomy between the two arms of the adaptive immune response led us to address how anti-HAdV antibodies influence anti-HAdV T-cell responses. In this study, we initially asked if healthy adults harbor HAdV-specific T_{regs}, which would be indicative of a path towards HAdV persistence. We then explored how tolerogenic DCs and HAdV-specific T_{regs} could be generated. We previously showed that IC-HAdV5s are internalized by, and aggregate in, DCs [14]. Following protein VI-dependent endosomal escape of the capsid, the viral genome is engaged by AIM2 in the cytoplasm. AIM2 nucleation induces ASC (apoptosis-associated speck protein containing a caspase activation/recruitment domain) aggregation, inflammasome formation, caspase 1 auto-activation, pro-IL-1β and GSDMD cleavage, and GSDMD-mediated loss of cell membrane integrity. Here we demonstrate that the pyroptotic environment induced by IC-HAdV5 plays a significant role the creation of tolerogenic bystander DCs. We further show that some of these bystander DCs can induce HAdV-specific memory T cells to proliferate, and/or drive naïve CD4 cells towards a T_{reg} phenotype. The T_{regs} generated in this *ex vivo* assay are capable of inhibiting the proliferation of anti-HAdV T cells. We therefore propose that an antiviral humoral responses can, counterintuitively, abet HAdV persistence.

Our assays using a human pathogen, naturally occurring human antibodies and primary blood-derived human cells address one possible immune cell-based mechanisms of adenovirus persistence. Yet, ex vivo results cannot unequivocally show causality. Host-pathogen-based studies have often used mice to address questions underlying disease-immune relationships. However, the impact of HAdVs on human and mouse DCs is notably different. Furthermore, we are unaware of studies directing addressing the impact of murine adenovirus (MAV) on murine DCs. In 1964, D. Ginder showed that a MAV can cause persistent infections for 10 weeks in outbred Swiss mice [50]. K. Spindler and colleagues then showed that MAV-1 infections persist for at least 55 weeks in outbred Swiss mice [51]. In addition, Spindler and colleagues demonstrated that in contrast to humans, mice that lack B cells are highly susceptible to MAV-1 infection, while mice that lack T cells are not susceptible [52]. In light of our results, the question could be raised as to whether anti-MAV-1 antibodies are needed to generate T_{regs} to reduce the potential impact T-cell induced immunopathology [27]. To address this one could use a single pre-injection of sera from MAV-1-challenged mice into B-cell deficient mice and quantify disease progression.

Using nonhuman primates (NHPs) to address the dichotomy between the two arms of the adaptive immune response to adenoviruses is likely a more informative option, but use of NHPs entails unique challenges when it comes to pre-existing exposure to their own set of adenoviruses. Nonetheless, Miller and colleagues showed that rhesus macaques harboring a neutralizing antibody response against a HAdV5 host-range mutant, and then re-challenged with the same virus, respond with a significant increase in circulating T_{regs} [53]. These *in vivo* observations, which hinge on pre-existing HAdV5 neutralizing antibodies, are consistent with our proposed mechanism. One also needs to take into account the dynamic, recurrent exposure to multiple HAdV types during childhood and adolescence. Although our study focused on HAdV5, a relatively common species C HAdV, we believe that recurrent exposure provides

numerous opportunities for the formation of IC-HAdVs, from multiple HAdV types, and the impetus to form cross-reactive HAdV T_{regs}.

Our data also complement the mechanism for HAdV persistence described by Hearing and colleagues [6]. Using human cell lines, they showed that IFN-α and IFN-γ production block HAdV5 replication via an E2F/Rb transcriptional repression of its E1A immediate early gene [54]. The E1A gene product is essential for activating expression of the other early genes and reprogramming the cell into a state that allows virus propagation. Of note, type 1 IFN secretion is significant from IC-HAdV5-challenged DCs and may allow HAdVs (including those that are covered with non-neutralizing Abs) to be taken up by neighboring cells to establish persistent infections.

Mechanisms by which DCs promote tolerance include induction of T_{regs}, the inhibition of memory T-cell responses, T-cell anergy, and clonal deletion [24–26]. The semi-mature phenotype of tolerogenic DCs provide insufficient stimulatory signals and drive naïve T cells to differentiate into T_{regs} rather than effector T cells [55]. The global anti-viral response by DCs acts via a combinatorial cytokine code to direct the response of neighboring immune cells. The cytokine profile produced by the IC-HAdV5-challenged DCs and bystander DCs is noteworthy, particularly in the context of the combination and dose that influences activation of other immune cells. Recently, a biochemical and functional chemokine interactome study suggested that several chemokines form heterodimers that have unique functions in certain conditions [56]. Based on these interactome data, we plotted the possible combinations that could influence the direct and bystander DCs in our assays (**S11 Fig**). What impact these heterodimers could have on HAdV persistence will require future study, in particular because we did not find notable levels of TGFβ secreted by direct or bystander DCs. More than other cytokine families, the IL-1 family may be primordial because it is tightly linked to IC-HAdV-induced DC pyroptosis. Indeed, the intracellular domain of the IL-1R1 shares similar signaling function properties with TLRs. In general, IL-1β release from monocytes is tightly controlled; less than 20% of the total pro-IL-1β precursor is processed and released. IL-1β also increases the expression of intercellular adhesion molecule-1 and vascular cell adhesion molecule–1, which, together with the chemokines, promote the infiltration of cells from the circulation into the extravascular space and then into inflamed tissues [57]. While circulating monocytes do not constitutively express *IL1β* mRNA, adhesion to surfaces during diapedesis induces the synthesis of large amounts that are assembled into large polyribosomes primed for translation [58].

At least two aspects of the IC-HAdV-induced DC immune response that remain unknown are the impact of neutrophils and the phenotype/function of recruited monocytes. Neutrophils are pertinent because they can secrete/release proteinase 3 (PR3), elastase, cathepsin-G, chymase, chymotrypsin, and meprin α or β, which can process extracellular pro-IL-1β into its active form [59,60]. In addition, IC-HAdVs activate neutrophils (L-selectin shedding) via Fc receptors and complement receptor 1 interactions [61]. Moreover, neutrophils are a major source for anti-microbial peptides (e.g., defensins and LL-37) and proteins (e.g. lactoferrin) for which a pro- or anti-viral roles in HAdV infection has been proposed [62]. With respect to the phenotype/function of recruited monocytes, $Ly6C^{hi}$ monocytes [63], which suppress T-cell proliferation during HAdV-induced inflammation [64], may also impact the creation of HAdV antigen-presenting tolerogenic DCs and HAdV-specific T_{regs}.

The dynamic equilibrium between recurrent HAdV infections and IC-HAdV formation, DC maturation/pyroptosis, recruitment and generation of bystander DC, and T_{regs} production/activation, likely starts in childhood and develops nonlinearly over decades. While it is hard to argue that the generation of persistent infections is not beneficial to the pathogen, it is possible that the sustained anti-HAdV cellular and humoral responses partially shield a healthy host from infections by other pathogens (e.g. hepatitis C virus [65]) or the related immune-

induced tissue damage [66]. Avoiding chronic tissue damage is particularly important because, as mentioned previously, HAdVs infect the eye, respiratory and gastrointestinal tracts. However, in a T-cell compromised host IC-HAdV-induced pyroptosis of $Fc\gamma R^+$ cells (neutrophils, monocytes, macrophages, DCs) may also prime the host for HAdV-disseminated disease.

In summary, our findings suggest a mechanism by which humoral immunity to HAdV fosters tolerance. Understanding this complex virus-host interplay may enable us to identify high risk patients undergoing immunosuppression and develop therapies to treat disseminated HAdV-disease [67,68].

Materials and methods

Ethics statement

Blood samples from anonymous donors (~120 from the Etablissement Français du sang, Montpellier, France, and 58 from Lausanne University Hospital/CHUV) were used during this study. All donors provided written informed consent.

Cells and culture conditions

DCs were generated from freshly isolated $CD14^+$ monocytes in the presence of 50 ng/ml granulocyte-macrophage colony-stimulating factor (GM-CSF) and 20 ng/ml interleukin-4 (IL-4) (PeproTech, Neuilly sur Seine, France) [3]. DC stimulations were performed 6 days post-isolation of monocytes. THP-1 cells purchased from ATCC (TIB-202) were cultured in RPMI 1640 medium supplemented with 10% fetal bovine serum (FBS). Similar to DCs, THP-1 cells were differentiated into DCs using 50 ng/ml GM-CSF and 20 ng/ml IL-4 for 6 days.

HAdV vectors & hexon peptides

Adβgal is a ΔE1/E3 HAdV5 vector harboring a *lacZ* expression cassette [69]. Ad^{L40Q} is an HAdV5-based vector with a leucine to glutamine mutation of an amino acid in protein VI that decreases its membrane lytic activity [31]. Alexa555- and Alexa488-HAdV5 were generated from Adβgal by using an Alexa555 or Alexa488 Protein Labeling Kit (Life Technologies, Villebon-sur-Yvette, France) as previously described [70]. Ad2ts1 harbors a mutation in protease and results in several unprocessed capsid proteins and a hyper-stable capsid [71]. All HAdV viruses/vectors were produced in 293 or 911 cells and purified by double banding on CsCl density gradients as previously describe [14]. Vector purity typically reaches >99%. HAdV concentrations (physical particles/ml) were determined as previously described [72]. The hexon peptide pool (PepTivator AdV5 hexon, Miltenyi) is overlapping sequences of the HAdV5 hexon protein.

Antibodies

Anti-human CD4-PE (cat 300508) was from BioLegend. Anti-human CD83-FITC (cat 556910), anti-human HLA-ABC-PE (cat 555553), anti-human HLA-DR-PE (cat 555812), anti-human CD80-FITC (cat 557226), anti-human CD86-APC (cat 555660), anti-human CD25-PE (cat 555432), anti-human CD127-FITC (cat 561697), anti-human CD4-PE-Cy7 (BD) (cat 348809), anti-TNF-PE-Cy7 (cat 557647), anti-human IL-2-PE (cat 559334), anti-human CD3-APC-H7 (cat 560176), anti-human CD4-CF594 (cat 5562281), anti-human CD4-PB (pacific blue), anti-human CD8-BV605 (cat 564116), anti-human CD8-PerCP-Cy5.5 (cat 341050), anti-human IFN-γ–AF700 (cat 557995), anti-human CD35-PE-Cy7 (cat 557741), anti-human IL-10 (cat 554707) were from Becton Dickinson, Pharmigen. Anti-human Foxp3-APC (cat 17-4776-41) was from eBioscience. Anti-human CD14-PE (cat A07764) was from Beckman

Coulter. Anti-human CD45RO-APC/Cy7 (cat 304227), anti-human CD45RA-PE (cat 304205), anti-human CD3-APC (cat 300411), and anti-human CD40-APC (cat 313008) were from BioLegend). Anti-human IL-10-BV421(cat 501421), anti-human CD45RA-BV711 (cat 304137), anti-human CD127-BV711 (cat 351327) from Biolegend, anti-human CD45RO-ECD (cat IM2712) (BC), anti-human FoxP3-PE (cat 12-4777-42), from eBiosciences.

Immune complex formation and DC stimulations

DCs (4 x 10^5 in 400 μl of complete medium) were incubated with HAdV5 or IC-HAdV5 (or IC) (2 x 10^4 physical particles (pp)/cell, unless otherwise indicated) for the indicated times. IC-HAdV5s were generated by mixing the virus (8 x 10^9 physical particles) with 2.5 μl of IVIg (human IgG pooled from 1,000 to 50,000 donors/batch) (Baxter SAS, Guyancourt, France) for 15 min at room temperature. IVIg is used in patients with primary or acquired immunodeficiency as well as autoimmune diseases. Z-VAD-FMK 20 μM (ZVAD) was added 2 h before stimulation. Brefeldin A was used at 3 μg/ml after 6 h stimulation or for the same time with stimulation.

Bystander DC stimulation

DCs (1.5 x 10^6 in 1.5 ml of full media) were incubated ± LPS 100 ng/ml, HAdV5, and IgG in the lower compartment of the well (12 mm diameter polyester membranes with 0.4 μm pores; (Corning, Bagneaux-sur-Loing, France). After 6 h incubation, fresh immature DCs (6 x 10^5 in 600 μl of media) were added to the upper compartment and are referred to as bystander DCs. TAK-242 was added to DCs 1 h pre-challenge.

Quantification of mRNA

Expression levels of cytokine and chemokine genes were evaluated using RT-qPCR assays. Total RNA was isolated from cells using the high pure RNA isolation Kit (Roche, Berlin, Germany) with a DNase I treatment during the purification and subsequent elution in 50 μl of RNase-free water (Qiagen, IN, USA). Reverse transcription was performed with the superscript first-strand synthesis system (Invitrogen) using 10 μl of total RNA and random hexamers. The cDNA samples were diluted 1:20 in water and analyzed in triplicate using a LightCycler 480 (Roche, Meylan, France). SYBR green PCR conditions were as follows: 95˚C for 5 min and 45 cycles of 95˚C for 15 s, 65˚C or 70˚C for 15 s, and 72˚C for 15 s using *GAPDH* as a standard. See **S2 Table** for primers sequencers. Relative gene expression levels of each respective gene were calculated using the threshold cycle ($2^{-\Delta\Delta CT}$) method and normalized to *GAPDH* mRNA levels.

RT^2 Profiler PCR array

Expression levels of cytokine and chemokine mRNAs were analyzed using PCR array assays. Total RNA was isolated from cells using the High Pure RNA isolation Kit (Roche, Berlin, Germany) with a DNase I treatment during the purification and elution in 50 μl of RNase-free water (Qiagen). Reverse transcription was performed with the RT^2 First strand Kit (Qiagen, Courtaboeuf, France), and the cDNA samples were analyzed in duplicate using a RT^2 Profiler ^{TM} PCR array (Qiagen). SYBR green PCR conditions were 95˚C for 10 min and 40 cycles of 95˚C for 15 s, and 60˚C for 1 min using 84 human inflammatory and receptor genes. The potential mRNAs were chosen and then confirmed by RT-qPCR.

The genes that contributed in each axis in the PCA were as follows: **F1** = *CCL1*, *2*, *4*, *5*, *7 13*, *15*, *17*, *20*, *22*, *CSF1*, *CX3CL1*, *CXCL 1 to 3*, *5*, *8 to 11*, *FASLG*, *IFNG*, *IL10RA*, *IL10RB*, *IL15*,

IL1a, *IL1b*, *IL7*, *NAMPT*, *TNFSF4*, *10*, *11*, *13*, *13B*, and *VEGFA*. **F2** = *AIMP1*, *C5*, *CCL1*, *2*, *13*, *17*, *23*, *CRR1*, *2*, *3*, *4*, *5*, *CSF1*, *CX3CR1*, *CXCR2*, *IL10RA*, *I10RB*, *IL15*, *LTA*, *LTB*, *MIF*, *SPP1*, *TNF*, *TNFSF4*, *10*, *11*, *13*, and *13B*. **F3** = *CCL17*, *23*, *CCR5*, *CX3CR1*, *IL10RA*, *IL5*, *IL9*, *MIF*, and *OSM*.

Co-stimulatory protein levels

Surface levels of CD83, MHCII, CD80, CD40, and CD86 were assessed by flow cytometry. Cell membrane integrity was assessed by collecting cells via centrifugation at 800x g; the cell pellets were then resuspended in PBS containing 10% FBS, propidium iodide (PI) (Sigma-Aldrich, Missouri, USA), or 7-aminoactinomycin D (7AAD) (Becton-Dickinson, New Jersey, USA). The cell suspension was incubated for the indicated times and analyzed using a FacsCalibur flow cytometer (Becton-Dickinson) and FlowJo software.

Intracellular staining

Surface and intracellular levels of CD83 and CD86 (total protein) were stained with a BD Cytofix/Cytoperm Fixation/Permeabilization Kit, and then measured by flow cytometry. To assess cell membrane integrity, the cells were collected and centrifuged at a speed of 800x g; the cell pellets were then resuspended in PBS, 10% FBS, PI (Sigma), or 7AAD and analyzed on a FacsCalibur flow cytometer (Becton-Dickinson) and FlowJo software.

Monocyte migration assay

Monocyte migration was evaluated using a 5.0 μm-diameter pore transwell system (Corning, Bagneaux-sur-Loing, France). Monocytes (2×10^5 in 200 μl of full media) were added into inserts and DCs or DCs (7.5×10^5 in 750 μl of full media) and ± LPS (100 ng/ml), HAdV5, HAd555, or IgG in the lower wells. Monocytes were stained by carboxy-fluorescein diacetate-succinimidyl ester (CFSE) (Molecular Probes, Eugene, OR, USA) (CellTrace CFSE Cell Proliferation Kit). DCs incubated for 30 min with HAd555 or HAdV5 and IgG in the lower chamber were or were not washed in medium before adding the stained CFSE monocytes. After 3, 6, and 24 h incubation at 37˚C, the cells in the upper and lower compartment were detected quantified using a FacsCalibur flow cytometer (Becton-Dickinson) and FlowJo software.

Cytokine secretion: ELISA and Luminex assays

Supernatant from the cells were collected and cytokine secretion was measured by ELISA and Luminex assays. The secretion of TNF and IL-1β was quantified by ELISA using an OptEIA human TNF ELISA Kit (Becton Dickinson) and human IL-1β/IL-1F2 DuoSet ELISA (R&D Systems, Lille, France) following the manufacturer's instructions. Additionally, 22 other cytokines and chemokines were detected by Luminex using a Bio-plex pro human chemokine, cytokine kit (Bio-Rad, Marnes-La-Coquette, France) following the manufacturer's instructions.

Depletion of $CD25^+$ from PBMCs

PBMCs were isolated using standard gradient separation techniques. Half were $CD25^+$-depleted, using anti-CD25 in a human $CD4^+CD25^+CD127^{dim/-}$ Regulatory T Cell Isolation Kit II and MACS separation system.

CFSE and VPD 450 labeling

PBMCs were washed and suspended in PBS for labeling with CFSE or Violet Proliferation Dye 450 (VPD 450) (BD Horizon, Le Pont de Claix, France) at a final concentration of 2.5 μM or 1 μM, respectively, for 3 min at room temperature. Labeling was terminated by the addition of fetal calf serum (FCS) (40% of total volume).

PBMC activation assays

PBMCs ± $CD25^+$ were stained with CFSE and cultivated in 96-well U-bottom plates; (cell concentration 1 x 10^6/ml and a final volume of 200 μl; PBMC $CD25^+$/ PBMC $CD25^-$ ratio 1:10). HAdV5 hexon peptides (PepTivator, Miltenyi, Paris, France) were added at 0.3 nmol. On days 3 and 5 the cells were split and IL-2 was added (final concentration 100 U/ml). Cells were analyzed on a FACS Canto II using FlowJo software.

T_{reg} generation

Naïve $CD4^+$ T cell were isolated using naïve $CD4^+$ T Cell Isolation Kit II and MACS separation system. DCs indirectly activated for 12 h with LPS, HAdV5, IC-HAdV5 and IgG, and then were co-cultured with $CD4^+$ naïve T cells labeled VPD450 (with ratio bystander DCs/ T cells is 3:1) in RPMI 1640 supplemented with 10% FCS and IL-2 (Proleukin 18 x 10^6 IU, CA, USA) (100 U/ml) for 3 or 7 days. Recombinant IL-2 was added on day 3 and day 5. CD25, CD127, and FoxP3 levels were quantified by flow cytometry using FACS Canto II.

Statistical analyses

All experiments were performed at least in duplicate a minimum of three independent times, and the results are expressed as mean ± SEM unless otherwise stated. The statistical analyses were performed using the Student's *t*-test unless otherwise stated. A p value < 0.05 is denoted as significant. Statistical analyses of the global cytokine profiles (pie chart) were performed by partial permutation tests using the SPICE software.

Supporting information

S1 Fig. Transwell assay setup and controls. A) We used transwell inserts with 0.4 um filter to generate direct and bystander DCs. Direct DCs (1.5 x10^6 cells unless mentioned otherwise) were incubated with the stimulus (e.g. LPS, HAdV5, mutant virus, ± IVIg ± drugs) in lower compartment for 6 h. Fresh DCs (6 x 10^5) were added to the upper compartment.
B) To determine if HAdV5 particles (2 x 10^4 pp/ml) added to the lower chamber diffused to the upper compartment and impact the bystander DCs, we quantified (by qPCR) HAdV5 genomes in the **supernatant** of each compartment. 1.6 x 10^{10} pp of HAdV5 pp were used in the control medium. These data demonstrate that 10,000-fold fewer particles could be found in the upper chamber.
C) Quantification of HAdV5 genomes **associated with bystander DCs** as measured by qPCR ($n \geq 3$). DNA from mock-treated samples was extracted and virus/cell was normalized to *GAPDH* copy number. The quantity of HAdV5 genomes/cell was normalized by *lacZ* (transgene in the vector) vs. *GAPDH* copy number. While direct DCs take up ~600 pp/cell [14], we found that 1 in 10 bystander DC contains a single HAdV5 genome.
D) The $7AAD^+$ bystander and direct DCs (i.e. DCs with compromised plasma membrane integrity) in each condition were quantified by flow cytometry. The assays were carried out in 4 donors (mean ± SEM. These results demonstrate that bystander DCs do not show loss of cell membrane integrity. p values were derived using Student's t-test (**B & C**) or one-way ANOVA

with Dunnett's post-tests (**D**). * $p < 0.05$, ** $p < 0.01$ and *** $p < 0.001$.
(TIF)

S2 Fig. Maturation/activation markers on bystander DCs. Bystander DCs were generated using milieu from DCs challenged with IgG, LPS, HAdV5, or IC-HAdV5. The color code is as in Fig 2. **A)** The data are representative flow cytometry profiles of CD40 and MHC II surface expression. A modest increase was noted in each case. **B)** In a dose-dependent assay (20,000, 5,000, or 1,000 pp/cell) CD86 cell surface levels were quantified detected by flow cytometry. The data are representative flow cytometry profiles. Assays were carried out in 4 donors with similar results. **C)** PCR array profiles from bystander DCs exposed to the milieu generated by DCs challenged by HAdV5, IC-HAdV5, and IC-Ad^{L40Q}. The 66 cytokine mRNAs that gave unique qPCR peaks in our hands. **D)** *IL1β*, *IL12p40*, *CLL3* and *IL6* mRNA levels in bystander THP1 DCs assayed in a dose-dependent (20,000, 10,000, 5,000, or 1,000 pp/direct DC) response. Data are mean ± SEM with 3 independent experiments. *p* values were derived from one-way ANOVA with Dunnett's test. * $p < 0.05$, ** $p < 0.01$ and *** $p < 0.001$.
(TIF)

S3 Fig. Bystander and direct DC cytokine mRNA levels as a function of time and dose. We extended the mRNA array results by quantifying dose-dependent responses of a handful of mRNA levels by RT-qPCR. Because DCs derived from monocytes from random blood bank donors can have widely different levels of mRNAs, we compared mRNA levels in THP-1-derived DCs to provide a standardized view of the changes. THP-1 cells were differentiated into DCs for 6 days, then directly and indirectly activated. **A)** *CCL3*, *IL1β*, and *IL6* mRNA levels in DCs challenged with LPS, IgG, HAdV5 and IC-HAdV5 (left hand column), and bystander DCs (right hand column) incubated in the respective direct DC milieu were quantified at 3, 6, and 18 h post-incubation. **B)** Changes in *TNF*, *IL1β*, IFN*β*, *IL6*, *and CCL3* mRNA levels in direct (left hand column)
TNF: IC 2 x 10^4 vs. 10^4 ns; 10^4 vs. 5 x 10^3 ns; 5 x 10^3 vs. x 10^3 ***; *IL1β* IC 2 x 10^4 vs. 10^4 ns; 10^4 vs. 5 x 10^3 ns; 5 x 10^3 vs. 10^3 ns; IC 2 x 10^4 vs. 10^3 **, IC 10^4 vs. 10^3 *;
IFNβ: IC 2 x 10^4 vs. 10^4 ns; 10^4 vs. 5 x 10^3 ns; 5 x 10^3 vs. 10^3 ns, IC 2 x 10^4 vs. 10^3 *; *IL6*: IC 2 x 10^4 vs. 10^4 ns; 10^4 vs. 5 x 10^3 **; 5 x 10^3 vs. 1 x 10^3 ns;
CCL3: IC 2 x 10^4 vs. 1 x 10^4 ns; 1 x 10^4 vs. 5 x 10^3 ***; 5 x 10^3 vs. 10^3 ns)
Bystander DC (right hand column) dose-dependent assay (2 x 10^4, 10^4, 5 x 10^3, or 10^3 pp/cell) by RT-qPCR
TNF: IC 2 x 10^4 vs. 10^4 ns; 10^4 vs. 5 x 10^3 ns; 5 x 10^3 vs. 1 k ns, IC 2 x 10^4 vs. 10^3 **, IC 10^4 vs. 10^3 ***;
IL1β: IC20 k vs. 10^4 ns; 10^4 vs. 5 x 10^3 ns; 5 x 10^3 vs. 10^3 ns;
IFNβ: IC 20 k vs. 10^4 ns; 10^4 vs. 5 x 10^3 ns; 5 x 10^3 vs. 10^3 **;
IL6: IC 2 x 10^4 vs. 10^4 ns; 10^4 vs. 5 x 10^3 ns; 5 x 10^3 vs. 10^3 ns, 10^4 vs. 5 x 10^3 ***;
CCL3: IC 2 x 10^4 vs. 10^4 ns; 10^4 vs. 5 x 10^3 ***; 5 x 10^3 vs. 10^3 *).
As in "**A**" controls included IgG and HAdV5.
Three independent experiments were carried out. Data are mean ± SEM. *p* values were derived using Student's *t*-tests. * $p < 0.05$, ** $p < 0.01$ and *** $p < 0.001$.
(TIF)

S4 Fig. Controls for ZVAD and brefeldin A assays. A) TNF and IL-1β secretion in response to ZVAD treatment (2 h before challenge) of DCs challenged with LPS, IgG, HAdV5, and IC-HAdV5.
B) DCs were simultaneously treated with brefeldin A and challenged with LPS, IgG, HAdV5, and IC-HAdV5. TNF secretion was quantified at 18 h.

C) DCs were simultaneously treated with brefeldin A and challenged with LPS, IgG, HAdV5, and IC-HAdV5. IL-1β secretion was quantified at 18 h. Data are mean ± SEM, *p* values were derived from Student's *t*-tests, n ≥ 3 donors. *** $p < 0.001$.
(TIF)

S5 Fig. Controls for IC-Ad^{L40Q} and IC-Ad2ts1. A) DCs challenged with LPS, IgG, HAdV5, Ad^{L40Q} and increasing concentrations of IC-HAdV5 and IC-Ad^{L40Q} were analyzed for loss of membrane integrity (7AAD^{+} cells), IL-1β and TNF secretion.
B) Cell surface levels of the maturation/activation markers CD86 and CD83 following direct DCs challenged with IgG, Ad^{L40Q}, IC-Ad^{L40Q}, HAdV5, and IC-HAdV5.
C) bystander DC *IL1β* and *IFNβ* mRNA levels quantified by RT-qPCR assay. Experiments were carried out in ≥3 donors. *p* values were derived from Student's *t*-tests. *, **, *** denote *p* values of < 0.05, < 0.01, < 0.001, respectively.
DCs were challenged with LPS, IgG, HAdV5, IC-HAdV5, Ad2ts1, and IC-Ad2ts1 and screened for **D)** time-dependent (6 to 48 h) TNF secretion; and **E)** time-dependent (6 to 48 h) loss of membrane integrity using propidium iodide (PI) incorporation; or
F) DCs were challenged with LPS, IgG, HAdV5, IC-HAdV5, Ad2ts1, and IC-Ad2ts1 and then used to generate bystander DCs in which the *IL1β* mRNA levels were quantified by RT-qPCR assay following dose-dependent stimulation (20 x 10^3, 10 x 10^3, or 5 x 10^3 pp/cell) of the direct DCs.
Experiments were carried out in 3 donors and in duplicate. *P* values were derived from Student's *t*-tests. ** $p < 0.01$.
(TIF)

S6 Fig. TAK-242 controls. Bystander DCs were treated with TAK-242 for 1 h before adding them to the DCs challenged with LPS, IgG, HAdV5, or IC-HAdV5. TNF secretion was quantified in direct DCs in the lower compartment (n = 3 donors). *p* values were derived from Student's *t*-tests. *** $p < 0.0001$.
(TIF)

S7 Fig. Controls for fluid phase uptake assay. Nonspecific binding of dextran to **A)** direct DCs and **B)** bystander DCs was controlled by incubating DC (post-stimulation) with FITC-labeled dextran at 4˚C. Direct DCs were challenged with IgG, LPS, HAdV5, or IC-HAdV5. The cells were then incubated with FITC-labeled dextran and analyzed by flow cytometry. The data are representative flow cytometry profiles with experiments performed using cells from in 3 donors and in duplicate.
(TIF)

S8 Fig. Controls for monocyte recruitment. A) A 5-micron-pore membrane transwell system was used for monocyte migration assays. The timing and stimuli are indicated in the schematics. Round green cells are CFSE-labeled monocytes. **B)** These data shown percentage of monocyte in the upper chamber that potentially interact with HAdV or IC-HAdV5. **C)** To address this possibility, we covalently linked Alex555 to the HAdV5 capsid (HAdV5-Alexa555 [29]) to identify cells associated with HAdV5 or IC-HAdV5. CFSE-labeled monocytes were then assayed by flow cytometry for loss of membrane integrity (7AAD^{+} cells) and the presence of HAdV5-Alexa555 at 6 and 24 h. These data demonstrate that ICs do not go through the pore to interact with monocytes in the upper chamber. **D)** CD14 expression levels on monocytes recruited towards bystander DCs that were created with the milieu from DCs challenged with IgG, LPS or HAdV5 at 24 h. **E)** CD14 and CD86 levels on monocytes recruited to bystander DCs that were created with the milieu from DCs challenged with IgG, LPS or HAdV5 at 72 h. **F)** CD14 and CD86 expression levels on monocytes that remained in the upper compartment

at 72 h. The lower compartment contained bystander DCs that were created with the milieu from DCs challenged with IgG, LPS or HAdV5. The data are representative flow cytometry profiles with assays carried out in 4 donors. * $p < 0.05$, ** $p < 0.01$ and *** $p < 0.001$.
(TIF)

S9 Fig. Bystander DCs, generated using the media from DCs challenged with IgG, HAdV5, and IC-HAdV5, were incubated with naive CD4^{+} T cells isolated from the same donors. Three days post-incubation we gated on CD127^{dim} cells to identify CD25^{+}/FoxP3^{high} cells. The data are representative flow cytometry profiles with assays carried out in 7 donors.
(TIF)

S10 Fig. Flow chart demonstrating the cells and process used for the T_{reg} assays.
(TIF)

S11 Fig. Potential cytokine heterodimer formation/interactions. Potential cytokine heterodimers are based on von Hundelshausen *et al.* [56] interactome data and the response generated by direct and bystander DCs.
(TIF)

S1 Table. Statistical analyses of bystander DC cytokine transcription profile.
(DOCX)

S2 Table. In-house designed primer sequences.
(DOCX)

Acknowledgments

We thank Sylvie Grandemange, Fabien Blanchet, Sebastian Nisole, Valerie Dardalhon, and Claire Daien for reagents and advice. We thank EKL members for technical help and constructive comments. We thank the MRI, member of the national infrastructure France-BioImaging, and SERENAD for statistical analyses.

Author Contributions

Conceptualization: Thi Thu Phuong Tran, Karsten Eichholz, Matthieu Perreau, Eric J. Kremer.

Data curation: Thi Thu Phuong Tran, Karsten Eichholz, Patrizia Amelio, Matthieu Perreau.

Formal analysis: Thi Thu Phuong Tran, Karsten Eichholz, Matthieu Perreau, Eric J. Kremer.

Funding acquisition: Eric J. Kremer.

Investigation: Eric J. Kremer.

Methodology: Thi Thu Phuong Tran, Karsten Eichholz, Matthieu Perreau, Franck J. D. Mennechet, Eric J. Kremer.

Project administration: Matthieu Perreau, Eric J. Kremer.

Resources: Crystal Moyer, Glen R. Nemerow.

Supervision: Eric J. Kremer.

Validation: Eric J. Kremer.

Visualization: Eric J. Kremer.

Writing – original draft: Eric J. Kremer.

Writing – review & editing: Eric J. Kremer.

References

1. Flomenberg P, Piaskowski V, Truitt RL, Casper JT. Characterization of human proliferative T cell responses to adenovirus. J Infect Dis. 1995; 171: 1090–1096. PMID: 7751682
2. Tang J, Olive M, Pulmanausahakul R, Schnell M, Flomenberg N, Eisenlohr L, et al. Human CD8+ cytotoxic T cell responses to adenovirus capsid proteins. Virology. 2006; 350: 312–322. https://doi.org/10.1016/j.virol.2006.01.024 PMID: 16499941
3. Perreau M, Kremer EJ. Frequency, Proliferation, and Activation of Human Memory T Cells Induced by a Nonhuman Adenovirus. J Virol. 2005; 79: 14595–14605. https://doi.org/10.1128/JVI.79.23.14595-14605.2005 PMID: 16282459
4. Lion T. Adenovirus infections in immunocompetent and immunocompromised patients. Clin Microbiol Rev. 2014; 27: 441–462. https://doi.org/10.1128/CMR.00116-13 PMID: 24982316
5. King CR, Zhang A, Mymryk JS. The persistent mystery of adenovirus persistence. Trends Microbiol. 2016; 24: 323–324. https://doi.org/10.1016/j.tim.2016.02.007 PMID: 26916790
6. Zheng Y, Stamminger T, Hearing P. E2F/Rb Family Proteins Mediate Interferon Induced Repression of Adenovirus Immediate Early Transcription to Promote Persistent Viral Infection. PLoS Pathog. 2016; 12: 1–24. https://doi.org/10.1371/journal.ppat.1005415 PMID: 26809031
7. Veltrop-Duits LA, Van Vreeswijk T, Heemskerk B, Thijssen JCP, Seady R El, Jol-Van Der Zijde EM, et al. High titers of pre-existing adenovirus serotype-specific neutralizing antibodies in the host predict viral reactivation after allogeneic stem cell transplantation in children. Clin Infect Dis. 2011; 52: 1405–1413. https://doi.org/10.1093/cid/cir231 PMID: 21628480
8. Leen AM, Sili U, Vanin EF, Jewell AM, Xie W, Vignali D, et al. Conserved CTL epitopes on the adenovirus hexon protein expand subgroup cross-reactive and subgroup-specific CD8+ T cells. Blood. 2004; 104: 2432–2440. https://doi.org/10.1182/blood-2004-02-0646 PMID: 15265797
9. Leen AM, Myers GD, Sili U, Huls MH, Weiss H, Leung KS, et al. Monoculture-derived T lymphocytes specific for multiple viruses expand and produce clinically relevant effects in immunocompromised individuals. Nat Med. 2006/09/26. 2006; 12: 1160–1166. https://doi.org/10.1038/nm1475 PMID: 16998485
10. Cichon G, Boeckh-Herwig S, Schmidt HH, Wehnes E, Muller T, Pring-Akerblom P, et al. Complement activation by recombinant adenoviruses. Gene Ther. 2001; 8: 1794–1800. https://doi.org/10.1038/sj.gt.3301611 PMID: 11803399
11. Mistchenko AS, Lenzi HL, Thompson FM, Mota EM, Vidaurreta S, Navari C, et al. Participation of immune complexes in adenovirus infection. Acta Paediatr. 1992; 81: 983–988. https://doi.org/10.1111/j.1651-2227.1992.tb12159.x PMID: 1290863
12. Mistchenko AS, Diez RA, Mariani AL, Robaldo J, Maffey AF, Bayley-Bustamante G, et al. Cytokines in adenoviral disease in children: association of interleukin-6, interleukin-8, and tumor necrosis factor alpha levels with clinical outcome. J Pediatr. 1994; 124: 714–720. doi:S0022347694000120 PMID: 8176557
13. Perreau M, Pantaleo G, Kremer EJ. Activation of a dendritic cell–T cell axis by Ad5 immune complexes creates an improved environment for replication of HIV in T cells. J Exp Med. 2008; 205: 2717–2725. https://doi.org/10.1084/jem.20081786 PMID: 18981239
14. Eichholz K, Bru T, Tran TTP, Fernandes P, Welles H, Mennechet FJD, et al. Immune-complexed adenovirus induce AIM2-mediated pyroptosis in human dendritic cells. PLoS Pathog. 2016; 12: e1005871. https://doi.org/10.1371/journal.ppat.1005871 PMID: 27636895
15. Schuurhuis DH, van Montfoort N, Ioan-Facsinay A, Jiawan R, Camps M, Nouta J, et al. Immune complex-loaded dendritic cells are superior to soluble immune complexes as antitumor vaccine. J Immunol. 2006; 176: 4573–4580. PMID: 16585547
16. Fernandes-Alnemri T, Yu J-W, Datta P, Wu J, Alnemri ES. AIM2 activates the inflammasome and cell death in response to cytoplasmic DNA. Nature. 2009; 458: 509–513. https://doi.org/10.1038/nature07710 PMID: 19158676
17. Bergsbaken T, Fink SL, Cookson BT. Pyroptosis: host cell death and inflammation. Nat Rev Microbiol. 2009; 7: 99–109. https://doi.org/10.1038/nrmicro2070 PMID: 19148178
18. Unterholzner L. The interferon response to intracellular DNA: Why so many receptors? Immunobiology. 2013; 218: 1312–1321. https://doi.org/10.1016/j.imbio.2013.07.007 PMID: 23962476
19. Shi J, Zhao Y, Wang K, Shi X, Wang Y, Huang H, et al. Cleavage of GSDMD by inflammatory caspases determines pyroptotic cell death. Nature. 2015; 526: 660–665. https://doi.org/10.1038/nature15514 PMID: 26375003

20. Belkaid Y. Regulatory T cells and infection: a dangerous necessity. Nat Rev Immunol. 2007; 7: 875–888. https://doi.org/10.1038/nri2189 PMID: 17948021

21. Raker VK, Domogalla MP, Steinbrink K. Tolerogenic dendritic cells for regulatory T cell induction in man. Front Immunol. 2015; 6: 1–11. https://doi.org/10.3389/fimmu.2015.00001

22. Li S, Gowans EJ, Chougnet C, Plebanski M, Dittmer U. Natural regulatory T cells and persistent viral infection. J Virol. 2008; 82: 21–30. https://doi.org/10.1128/JVI.01768-07 PMID: 17855537

23. Yadav M, Stephan S, Bluestone JA. Peripherally induced Tregs-role in immune homeostasis and autoimmunity. Front Immunol. 2013; 4: 1–12. https://doi.org/10.3389/fimmu.2013.00001

24. Lutz MB, Schuler G. Immature, semi-mature and fully mature dendritic cells: Which signals induce tolerance or immunity? Trends in Immunology. 2002. pp. 445–449. https://doi.org/10.1016/S1471-4906(02)02281-0 PMID: 12200066

25. Ma Y, Shurin G V., Gutkin DW, Shurin MR. Tumor associated regulatory dendritic cells. Seminars in Cancer Biology. 2012. pp. 298–306. https://doi.org/10.1016/j.semcancer.2012.02.010 PMID: 22414911

26. Kanamori M, Nakatsukasa H, Okada M, Lu Q, Yoshimura A. Induced regulatory T cells: their development, stability, and applications. Trends Immunol. 2016; 37: 803–811. https://doi.org/10.1016/j.it.2016.08.012 PMID: 27623114

27. Josefowicz SZ, Lu LF, Rudensky AY. Regulatory T cells: mechanisms of differentiation and function. Annu Rev Immunol. 2012; 30: 531–564. https://doi.org/10.1146/annurev.immunol.25.022106.141623 PMID: 22224781

28. Iberg CA, Jones A, Hawiger D. Dendritic cells as inducers of peripheral tolerance. Trends in Immunology. 18 Aug 2017: 1–12. https://doi.org/10.1016/j.it.2017.07.007 PMID: 28826942

29. Perreau M, Mennechet F, Serratrice N, Glasgow JN, Curiel DT, Wodrich H, et al. Contrasting effects of human, canine, and hybrid adenovirus vectors on the phenotypical and functional maturation of human dendritic cells: implications for clinical efficacy. J Virol. 2007; 81: 3272–3284. https://doi.org/10.1128/JVI.01530-06 PMID: 17229706

30. Domogalla MP, Rostan P V., Raker VK, Steinbrink K. Tolerance through education: How tolerogenic dendritic cells shape immunity. Frontiers in Immunology. 2017. https://doi.org/10.3389/fimmu.2017.01764 PMID: 29375543

31. Moyer CL, Wiethoff CM, Maier O, Smith JG, Nemerow GR. Functional genetic and biophysical analyses of membrane disruption by human adenovirus. J Virol. 2011; 85: 2631–2641. https://doi.org/10.1128/JVI.02321-10 PMID: 21209115

32. Mangel WF, San Martin C. Structure, function and dynamics in adenovirus maturation. Viruses. 2014; 6: 4536–4570. https://doi.org/10.3390/v6114536 PMID: 25421887

33. Ortega-Esteban A, Bodensiek K, San Martín C, Suomalainen M, Greber UF, de Pablo PJ, et al. Fluorescence tracking of genome release during the mechanical unpacking of single viruses. ACS Nano. 2015; 24: 10571–9. https://doi.org/10.1021/acsnano.5b03020

34. Ohashi K, Burkart V, Flohe S, Kolb H. Cutting Edge: Heat shock protein 60 is a putative endogenous ligand of the toll-like receptor-4 complex. J Immunol. 2000; 164: 558–561. https://doi.org/10.4049/jimmunol.164.2.558 PMID: 10623794

35. Roelofs MF, Boelens WC, Joosten L, Abdollahi-Roodsaz S, Geurts J, Wunderink LU, et al. Identification of small heat shock protein B8 (HSP22) as a novel TLR4 ligand and potential involvement in the pathogenesis of rheumatoid arthritis. J Immunol. 2006; 176: 7021–7027. https://doi.org/10.4049/jimmunol.176.11.7021 PMID: 16709864

36. Park JS, Gamboni-Robertson F, He Q, Svetkauskaite D, Kim J-Y, Strassheim D, et al. High mobility group box 1 protein interacts with multiple Toll-like receptors. Am J Physiol Cell Physiol. 2006; 290: C917—C924. https://doi.org/10.1152/ajpcell.00401.2005 PMID: 16267105

37. Rallabhandi P, Phillips RL, Marina S. Respiratory syncytial virus fusion protein-induced toll-like receptor 4 (TLR4) signaling is inhibited by the TLR4 antagonists rhodobacter sphaeroides lipopolysaccharide and eritoran (e5564) and requires direct interaction with MD-2. MBio. 2012; 3: e00218—12. https://doi.org/10.1128/mBio.00218-12 PMID: 22872782

38. Shimazu R, Akashi S, Ogata H, Nagai Y, Fukudome K, Miyake K, et al. MD-2, a molecule that confers lipopolysaccharide responsiveness on toll-like receptor 4. J Exp Med. 1999; 189: 1777–1782. https://doi.org/10.1084/jem.189.11.1777 PMID: 10359581

39. Deguchi A, Tomita T, Omori T, Komatsu A, Ohto U, Takahashi S, et al. Serum amyloid A3 binds MD-2 to activate p38 and NF-κB pathways in a MyD88-dependent manner. J Immunol. 2013; 191: 1856–1864. https://doi.org/10.4049/jimmunol.1201996 PMID: 23858030

40. Hiratsuka S, Watanabe A, Sakurai Y, Akashi-Takamura S, Ishibashi S, Miyake K, et al. The S100A8-serum amyloid A3-TLR4 paracrine cascade establishes a pre-metastatic phase. Nat Cell Biol. 2008; 10: 1349–1355. https://doi.org/10.1038/ncb1794 PMID: 18820689

41. Eichholz K, Mennechet FJD, Kremer EJ. Human coagulation factor X-adenovirus type 5 complexes poorly stimulate an innate immune response in human mononuclear phagocytes. J Virol. 2015; 89: 2884–2891. https://doi.org/10.1128/JVI.03576-14 PMID: 25540380

42. Sallusto F, Cella M, Danieli C, Lanzavecchia A. Dendritic cells use macropinocytosis and the mannose receptor to concentrate macromolecules in the major histocompatibility complex class II compartment: downregulation by cytokines and bacterial products. J Exp Med. 1995; 182: 389–400. https://doi.org/10.1084/jem.182.2.389 PMID: 7629501

43. Min WP, Zhou D, Ichim TE, Strejan GH, Xia X, Yang J, et al. Inhibitory feedback loop between tolerogenic dendritic cells and regulatory T cells in transplant tolerance. J Immunol. 2003; 170: 1304–1312. https://doi.org/10.4049/jimmunol.170.3.1304 PMID: 12538690

44. Shi C, Pamer EG. Monocyte recruitment during infection and inflammation. Nat Rev Immunol. 2011; 11: 762–774. https://doi.org/10.1038/nri3070 PMID: 21984070

45. Danella Polli C, Alves Toledo K, Franco LH, Sammartino Mariano V, de Oliveira LL, Soares Bernardes E, et al. Monocyte migration driven by galectin-3 occurs through distinct mechanisms involving selective interactions with the extracellular matrix. ISRN Inflamm. 2013; 2013: 259256. https://doi.org/10.1155/2013/259256 PMID: 24049657

46. Jakubzick C V., Randolph GJ, Henson PM. Monocyte differentiation and antigen-presenting functions. Nat Rev Immunol. 2017; 17: 349–362. https://doi.org/10.1038/nri.2017.28 PMID: 28436425

47. Perreau M, Kremer EJ. The conundrum between immunological memory to adenovirus and their use as vectors in clinical gene therapy. Mol Biotechnol. 2006; 34: 247–256. https://doi.org/10.1385/MB:34:2:247 PMID: 17172670

48. Perreau M, Guérin MC, Drouet C, Kremer EJ. Interactions between human plasma components and A xenogenic adenovirus vector: Reduced immunogenicity during gene transfer. Mol Ther. 2007; 15: 1998–2007. https://doi.org/10.1038/sj.mt.6300289 PMID: 17712332

49. Leen AM, Christin A, Khalil M, Weiss H, Gee AP, Brenner MK, et al. Identification of hexon-specific CD4 and CD8 T-cell epitopes for vaccine and immunotherapy. J Virol. 2008; 82: 546–554. https://doi.org/10.1128/JVI.01689-07 PMID: 17942545

50. Ginder DR. Increased susceptibility of mice infected with mouse adenovirus to Escherichia coli-induced pyelonephritis. J Exp Med. 1964; 120: 1117–28. Available: http://www.ncbi.nlm.nih.gov/pubmed/14238929 PMID: 14238929

51. Smith K, Brown CC, Spindler KR. The role of mouse adenovirus type 1 early region 1A in acute and persistent infections in mice. J Virol. 1998; 72: 5699–706. Available: http://www.ncbi.nlm.nih.gov/pubmed/9621028 PMID: 9621028

52. Moore ML, McKissic EL, Brown CC, Wilkinson JE, Spindler KR. Fatal disseminated mouse adenovirus type 1 infection in mice lacking B cells or Bruton's tyrosine kinase. J Virol. 2004; 78: 5584–90. https://doi.org/10.1128/JVI.78.11.5584-5590.2004 PMID: 15140955

53. Qureshi H, Genesca M, Fritts L, McChesney MB, Robert-Guroff M, Miller CJ. Infection with host-range mutant adenovirus 5 suppresses innate immunity and induces systemic CD4+ T cell activation in rhesus macaques. PLoS One. 2014; 9: e106004. https://doi.org/10.1371/journal.pone.0106004 PMID: 25203111

54. Berk AJ. Recent lessons in gene expression, cell cycle control, and cell biology from adenovirus. Oncogene. 2005. pp. 7673–7685. https://doi.org/10.1038/sj.onc.1209040 PMID: 16299528

55. Banchereau J, Briere F, Caux C, Davoust J, Lebecque S, Liu YJ, et al. Immunobiology of dendritic cells. Annu Rev Immunol. 2000; 18: 767–811. https://doi.org/10.1146/annurev.immunol.18.1.767 PMID: 10837075

56. von Hundelshausen P, Agten SM, Eckardt V, Blanchet X, Schmitt MM, Ippel H, et al. Chemokine interactome mapping enables tailored intervention in acute and chronic inflammation. Sci Transl Med. 2017; 9: 1–15. https://doi.org/10.1126/scitranslmed.aah6650 PMID: 28381538

57. Nourshargh S, Renshaw SA, Imhof BA. Reverse migration of neutrophils: where, when, how, and why? Trends Immunol. 2016; 37: 273–286. https://doi.org/10.1016/j.it.2016.03.006 PMID: 27055913

58. Schindler R, Clark B, Dinarello C. Dissociation between interleukin-1 beta mRNA and protein synthesis in human peripheral blood mononuclear cells. J Biol Chem. 1990; 265: 10232–7. PMID: 2354999

59. Netea MG, van de Veerdonk FL, van der Meer JWM, Dinarello CA, Joosten LAB. Inflammasome-Independent Regulation of IL-1-Family Cytokines. Annu Rev Immunol. 2015; 33: 49–77. https://doi.org/10.1146/annurev-immunol-032414-112306 PMID: 25493334

60. Coeshott C, Ohnemus C, Pilyavskaya A, Ross S, Wieczorek M, Kroona H, et al. Converting enzyme-independent release of tumor necrosis factor alpha and IL-1beta from a stimulated human monocytic cell line in the presence of activated neutrophils or purified proteinase 3. Proc Natl Acad Sci U S A. 1999; 96: 6261–6266. https://doi.org/10.1073/pnas.96.11.6261 PMID: 10339575

61. Cotter MJ, Zaiss AK, Muruve DA. Neutrophils interact with adenovirus vectors via Fc receptors and complement receptor 1. J Virol. 2005; 79: 14622–14631. https://doi.org/10.1128/JVI.79.23.14622-14631.2005 PMID: 16282462

62. Wilson SS, Bromme BA, Holly MK, Wiens ME, Gounder AP, Sul Y, et al. Alpha-defensin-dependent enhancement of enteric viral infection. PLOS Pathog. 2017; 13: e1006446. https://doi.org/10.1371/journal.ppat.1006446 PMID: 28622386

63. Menezes S, Melandri D, Anselmi G, Perchet T, Loschko J, Dubrot J, et al. The heterogeneity of Ly6Chi monocytes controls their differentiation into iNOS+ macrophages or monocyte-derived dendritic cells. Immunity. 2016; 45: 1205–1218. https://doi.org/10.1016/j.immuni.2016.12.001 PMID: 28002729

64. Zhu J, Chen H, Huang X, Jiang S, Yang Y. Ly6Chi monocytes regulate T cell responses in viral hepatitis. JCI Insight. 2016; 1: 1–12. https://doi.org/10.1172/jci.insight.89880 PMID: 27777980

65. Singh S, Vedi S, Samrat SK, Li W, Kumar R, Agrawal B. Heterologous immunity between adenoviruses and hepatitis C virus: A new paradigm in HCV immunity and vaccines. PLoS One. 2016; 11: e0146404. https://doi.org/10.1371/journal.pone.0146404 PMID: 26751211

66. Medzhitov R, Durieux J, Wolff S, Dillin A, Prahlad V, Cornelius T, et al. Disease tolerance as a defense strategy. Science (80-). 2012; 335: 936–941. https://doi.org/10.1126/science.1214935 PMID: 22363001

67. Mynarek M, Ganzenmueller T, Mueller-Heine A, Mielke C, Gonnermann A, Beier R, et al. Patient, virus, and treatment-related risk factors in pediatric adenovirus infection after stem cell transplantation: Results of a routine monitoring program. Biol Blood Marrow Transplant. 2014; 20: 250–256. https://doi.org/10.1016/j.bbmt.2013.11.009 PMID: 24269896

68. Feghoul L, Chevret S, Cuinet A, Dalle JH, Ouachée M, Yacouben K, et al. Adenovirus infection and disease in paediatric haematopoietic stem cell transplant patients: Clues for antiviral pre-emptive treatment. Clin Microbiol Infect. 2015; 21: 701–709. https://doi.org/10.1016/j.cmi.2015.03.011 PMID: 25882354

69. Kremer EJ, Boutin S, Chillon M, Danos O. Canine adenovirus vectors: an alternative for adenovirus-mediated gene transfer. J Virol. 2000; 74: 505–512. https://doi.org/10.1128/JVI.74.1.505–512.2000 PMID: 10590140

70. Soudais C, Boutin S, Hong SS, Chillon M, Danos O, Bergelson JM, et al. Canine adenovirus type 2 attachment and internalization: coxsackievirus-adenovirus receptor, alternative receptors, and an RGD-independent pathway. J Virol. 2000; 74: 10639–10649. https://doi.org/10.1128/Jvi.74.22.10639–10649.2000 PMID: 11044108

71. Imelli N, Ruzsics Z, Puntener D, Gastaldelli M, Greber UF. Genetic reconstitution of the human adenovirus type 2 temperature-sensitive 1 mutant defective in endosomal escape. Virol J. 2009/10/29. 2009; 6: 174. https://doi.org/10.1186/1743-422X-6-174 PMID: 19860872

72. Mittereder N, Yei S, Bachurski C, Cuppoletti J, Whitsett JA, Tolstoshev P, et al. Evaluation of the efficacy and safety of in vitro, adenovirus-mediated transfer of the human cystic fibrosis transmembrane conductance regulator cDNA. Hum Gene Ther. 1994; 5: 717–729. https://doi.org/10.1089/hum.1994.5.6-717 PMID: 7948134